# Delft University of Technology

## Additional Thesis

---

## A Physics-Based approach for Rating Curves to Reduce Uncertainties
### A New Concept for Hydrological Model Calibration

---

*Author:*
Bart Strijker

*Supervisors:*
Prof. dr. ir. H.H.G. Savenije [1]
Ir. W.M.J. Luxemburg [1]

Wednesday 27th September, 2017

---

[1] Department of Hydrology, Faculty of Civil Engineering and Geosciences, Delft University of Technology

*As to methods, there may be a million and then some, but principles are few. The man who grasps principles can successfully select his own methods. The man who tries methods, ignoring principles, is sure to have trouble.*

Harrison Emmerson (1911)

# Acknowledgements

# Abstract

The direct measurement of discharges in rivers can be time-consuming and costly. The discharge is commonly estimated indirectly by means of a curve, relating water level to discharge. This so-called rating curve is traditionally determined by fitting a curve to a number of observations, which induces several uncertainties and difficulties: 1) the curve is approximated by a function type, 2) in general there are no observations for high flow conditions and 3) it needs to updated regularly due to cross sectional changes.

In this research a physics-based rating curve is developed and evaluated that is more reliable and easy to update. By the use of a photogrammetry techtnique 3D surface maps of river banks are generated by pictures obtained from an Unmanned Aerial Vehicle (UAV). The topography of the main channel is determined by using an Acoustic Doppler Current Profiler (ADCP) or it is approximated by the making use of expert judgement and the method developed by Lane (relates the water depth of the channel to the width and natural angle of repose). By knowing the geometric profile of a river reach, only the roughness coefficient and water surface slope are the unknown parameters to derive the rating curve, where the Manning's formula acts as the basis of the rating curve. In this way, the rating curves can be made physically substantiated and the calibration parameter is the combination of roughness and water surface slope.

Instead of using the power law function as a approximate function of the rating curve, it is used as approximation of the conveyance-water level relationship. Therefore, the exponents in the power law function are physical substantiated and reduce uncertainties in the extrapolation zone of the traditional method, because the profile during high flow conditions is also known. Further more, the local invariabilities that are specific to single cross-section analyses are minimized by analysing river reaches. It is demonstrated that local invariabilities arises easily in natural rivers that are causing non-uniform flows, which make in general the the open-channel flow analysis much more complex. However, the average conveyance of a reach may led to the a valid assumption of a uniform flow (which is part of the assumption in the Manning's formula), depending on how the local variabilities behave. The calibration of rating curves are much easier compared with the traditional way. Instead of collecting new discharge measurements during dispersed flows, you just have to visit the area ones with a drone and surveying equipment. During this visit, the new new geometric profile can be captured and the rating curve can be updated, assuming that the roughness and water surface slope remains constant.

# Contents

# List of Figures

## List of Tables

# 1 Introduction

## 1.1 Motivation

The direct measurement of discharges in rivers can be time-consuming and costly. The discharge is commonly estimated indirectly by means of a curve, relating water level to discharge. This so-called rating curve is traditionally determined by fitting a curve to a number of observations (discharge and water level), which are measured during a certain time period in a certain cross section of a river at a fixed geographical location. The precision and overall accuracy of these rating curves influences the ability to correctly describe flow regimes. There are three main reasons why the traditional method of curve fitting the fall short.

Firstly, the relationship between water level and discharge is approximated by a function type, which is in most cases the power law function. The three unique parameters of this function are based on curve fitting to the series of observations, which assumes that the water level and discharge relationship has a particular form. Even though the power law function is the most used function, several studies showed that this often leads to inaccurate estimates of full range of flows(Parodi & Ferraris, 2004; Petersen-Øverleir, 2006).

Subsequently, there are usally no observations obtained under high flow conditions due to difficulties in the measurement process: areas are hardly reachable and the conditions to be in and around a river are hazardous. The consequence is that a great part of the rating curve is based on extrapolation. The extrapolation of this assumed function induces uncertainties and probably errors in the rating curve (Kuczera, 1996), which particularly occur during the extreme conditions of the hydrological system. These conditions are especially interesting for hydrologists, because of water resources assessment and flood forecasting. Also the extrapolation in low flows lead to uncertainties, which in most cases occupies a large part of an annual hydrograph (Petersen-Øverleir, Asgeir, 2014). The characteristics of low-flow play a key role in for example drought analysis.

Thirdly, observations represent snapshots of the river state at one particular cross section and may be exposed to cross section changes due to vegetation growth and/or bad and bank movements, particularly during floods. This means that the relationship between water level and discharge may be non-stationary in time (Freer, McMillan, McDonnell & Beven, 2004). Therefore the rating curve needs to be updated regularly, depending on the dynamics of the river. The traditional method requires several observations, which needs to be preferable collected during dispersed flows in the river. The fact that one discharge measurement is time-consuming and the preferable dispersed flow measurements makes the composition of a rating curve even more time-consuming.

### 1.1.1 Hydrological model calibration: room for improvement

The importance of reliable rating curves, that describe the relation between water levels and discharges properly for low and high discharges, is that hydrographs (discharge versus time) are commonly used as a calibration parameter for a hydrological model. The rating curve is the tool to transfer the measured water levels to the corresponding hydrograph and therefore errors in this rating curve result in errors in the observed hydrograph. In hydrological modelling this observed hydrograph is compared with the modelled hydrograph to check its performance and to calibrate model parameters. Models with an inaccurate observed hydrograph leads to biased model parameters and thus to a biased hydrological model.

A new approach is developed whereby conceptual rainfall-runoff models are calibrated on the basis of water level data only. This new approach excludes indirectly unreliable discharge measurements in the calibration process by introducing extra conceptual model parameters to define the rating curve, which need to be calibrated and optimized in the hydrological model. A stepwise calibration method is applied, whereby first the rating curves parameters and then the remaining model parameters are estimated. This calibration method still contains uncertainties resulting from coefficients in the rating curve. However, these coefficients have physical properties and could be determined in a more justified

approach.

When hydrologists make use of hydrometric data for modelling applications, discharge uncertainty is always present, and becomes influential during calibration and validation. Several studies comprise in which error models for discharge have been justified and included (Pappenberger et al., 2006; Huard and Mailhot, 2008; Liu et al., 2009; Krueger et al., 2010a; McMillan et al., 2010; Westerberg et al., 2011). These studies focus on quantifying uncertainties, which in the first place makes hydrological modelling more reliable. In the second place it reduces uncertainties to base the hydrological models actually on reality.

Indirect measurements of discharges beyond the measurement range should rely on a physically based model rather than on the traditional approach of extrapolating rating curves based on analytical relationships. Also interpolation between several pairs of discharge and water level in the rating curve could be improved. A hydraulic analysis of the river reach is allowed nowadays by the broad availability of topographic data and new techniques in surveying to frame a physically based model. The geometry of river reaches can be determined by 3D photo-based surface maps. The use of imagery from Unmanned Aerial Vehicles (UAVs) can result in ultra-high resolution digital maps and can be acquired in much shorter time intervals than would be normally achievable through conventional grid mapping (Bemis et al., 2014). This may help to substantiate the coefficients in the rating curves based on physical properties of a river reach (Di Baldassarre & Claps, 2011) and lead to reduction of discharge uncertainties in the calibration process of hydrological models.

### 1.1.2 Research contribution: Usage of remote sensing techniques in hydrological model

There is a worldwide trend towards reducing the number of locations where streamflow is actively monitored (Brown, 2002) and drainage basins in many parts of the world are ungauged or poorly gauged (Sivapalan, 2003). This tendency for reducing monitoring locations comes at the same time as an increase in the interest in terrestrial hydrology and streamflow due to their roles in changes in flood frequency and water resource assessment associated with climatic changes. There is clearly a need to develop methods to facilitate the monitoring of streamflow that require little time "in the field" and are both cost effective and safe.

Various satellites yield valuable spatio-temporal information such is land surface elevation, water levels and water surface slope (Alsdorf, Rodríguez & Lettenmaier, 2007). Instead of measuring water levels in situ, there can be made use of overpassing satellites and their equipment. Radar altimeters show great promise for directly measuring water level variation in medium/large rivers (Smith, 1997), which have a vertical elevation accuracy of 10 cm at best and is usually 50 cm (Yan, Di Baldassarre, Solomatine & Schumann, 2015). The accuracy varies, depending on distance between the altimetry observation and the ground, and on the topography and the width of the river (Michael Durand, 2014). In ungauged and poorly gauged basins, there is a lack of concurrent data at multiple space-time scales for hydraulic (Yan et al., 2015) and hydrological modelling(Schaefli, Harman, Sivapalan & Schymanski, 2011).

The location where the groundtrack of a satellite orbit crosses the reach of a river can be seen as a virtual gauge. The difficulty nowadays is that the satellite will not overpass sequentially at the same location every repeat cycle, so neither be the virtual gauges at the same location. Discrepancies between altimetry and in situ measurements might be very high, because of the distance between the virtual station (VS) and the ground-based gauging station. This limitation can be reduced with simple 1D or 2D hydraulic models. Water levels at virtual stations can be transformed to water levels at gauging stations, where the rating curves are known.

Remote sensing techniques are also used to determine inundation areas of rivers. Those are generally estimated from optical or microwave satellite imagery, while water levels are obtained from satellite-borne radar or lidar data: two different remote sensing techniques, which are nowadays installed on different satellites. A new NASA mission, Surface Water and Ocean Topography (SWOT), will be capable of measuring key hydraulic variables associated with rivers, lakes, wetlands, and reservoirs by

combining different radar equipment on the same satellite (Lee-Lueng, Douglas, Rosemary & Ernesto, 2013). The launch is currently planned for April 2021 and scientists hope the measurements it takes as it circles the globe every 11 days will help track floods, monitor droughts, and protect livelihoods. However, ground-based river discharge measurements are still required to develop the rating curves and the accuracy of those remotely sensed data is still insufficient to use them to determine Digital Elevation Maps (DEM) to describe the complete geometry of small and medium rivers. There is a lot of potential of satellite data, where this research project could contribute to.

## 1.2 Aims and objectives

The calibration process of hydrological models may yield biased parameter estimates, which leads to biased hydrological models. Predictions of catchment responses and the understanding of hydrological cycles are challenges that could be made more reliable by reducing errors in the calibration process. This can be done by extending the model calibration technique, which is based on water levels only. In addition, extra parameters will be included to the calibration method which describes the rating curve and are physically based. This research takes one step towards that overall goal and the aim of the research presented in this thesis is:

> Develop and evaluate a physics-based rating curve that captures the geometric profile of a river reach in order to reduce uncertainties.

The calibration process will rely more on a physically based approach rather than the traditional approach based on an analytical relationship. Adding the the geometric profile of the river, which significantly influence the stream flow in a river reach (Di Baldassarre & Claps, 2011), will reduce several uncertainties. The curves will be more fundamentally for regular flow circumstances and are more reliable in the extrapolation zones of the rating curves. This new calibration method should make it easier to calibrate the rating curves in a river. The uncertainty in the rating curve can be reduced and this new calibration method could be more accessible to compose rating curves.

In addition, for the development and understanding of the potential of the physically based calibration process, the following specific objectives are defined:

1. **Physical substantiation of exponents in the power law function**, that approximate the rating curve, which depends on the shape of the river profile. This can be done by analysing the entire river profile, instead of curve fitting to observations obtained during regular flow circumstances. An approximation of exponents based on the geometry of the river reach is a more feasible option with regard to uncertainties in the inter- and extrapolation zone of the traditional method.

2. **Minimizing the local invariabilities that is specific to single cross-sections**, by analysing river reaches, instead of one cross-section. Reach averaged values can be derived from a 3D surface map of a river reach, which suppose to be less sensitive to changes in the cross-section. This ensures a longer validity of the rating curves and levelling out the local invariabilities also reduce the probability of non-uniformities in river reaches as with an one cross-section.

3. **Initiating an accessible method to calibrate rating curves**, because of the limited validity due to scouring and redeposition of river profiles. Time variant cross-sections ensure that the rating curves needs to be calibrated regularly, especially in the case of dynamic rivers. However, the traditional approach has the disadvantage that calibration the rating curve is a time-consuming task and is often done once in several years. This new method should make it easier to establish the calibration of rating curves.

## 1.3 Structure report

This section gives an overview of the report structure, and with that a short overview of the methods used to achieve the aim and objective of this research. The report is divided into chapters, where each chapter consists of sections of which some are subdivided into subsections.

After this introduction, the context of the research is described in chapters 2 and 3. Chapter 2 provides a short overview of the locations where this new calibration technique is tested. Chapter 3 will give relevant background knowledge about the current method and limitations and introduces a new physics-based approach. The methodology is described in Chapter 4 by treating the used equipment for data collection and its processing procedure to obtain 3D surface reconstruction. The performed terrain analysis of these surface maps are elaborated. Chapter 5 is the chapter on results and will show the outcomes of the terrain analysis and the resulting physics-based rating curve. Then in chapter 6 the investigation of this report are discussed and the strong and weak points of the research are pointed out. The main findings of this research are listed in the chapter 7 and there made recommendations about the implementation of the reports findings and potential further research or development on this topic in chapter 8.

## 2 Area description

### 2.1 Locations of case study

The new approach is demonstrated in several rivers in the Zambezi river basin. This basin extends over 1.390.000 km² and drains eight southern African countries, namely, Angola, Botswana, Malawi, Mozambique, Namibia, Tanzania, Zambia and Zimbabwe. The measurements are done in several rivers in the Middle Zambezi basin in the northern part of Zimbabwe (see figure 1).

Zimbabwe consists of a watershed plateau (highveld) about 1500–2000 m above sea level running roughly south west to north east. An escarpment north west separates the plateau and the lowveld Zambezi valley and the climate of this area is characterised by four seasons. These are spring (September to October), summer (November to April), autumn (April to June), and winter (July to August). The rainy seasons are short, usually spanning from November to April, with average rainfall of about 768mm and a mean temperature of 31 ºC. The expected flow of Zimbabwean rivers varies significantly from season to season. This research focusses on 4 rivers and their catchments in the North of Zimbabwe, namely Rukomechi river, Angwa river, Manyame river and Musengezi river (respectively from left to right in figure 1). Table 1 gives an overview of the gauging stations and different catchments areas.
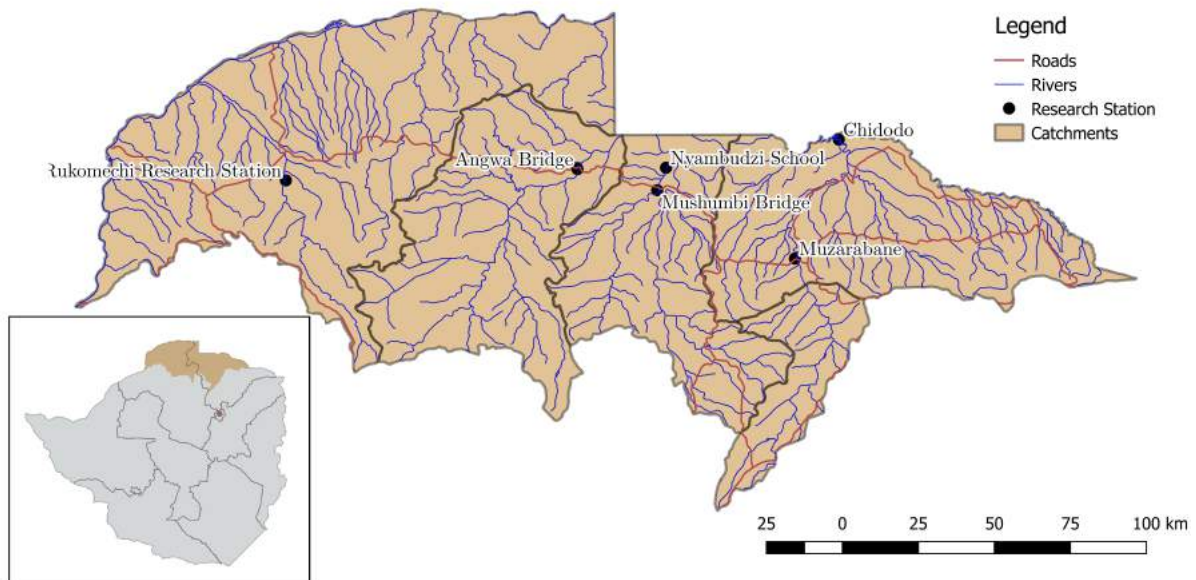


Figure 1: Location of the area under study.

Table 1: Overview of the research stations and their catchment

| Gauging station | Catchment |
|---|---|
| Angwa Bridge | Lower Angwa |
| Nyambudzi School | Lower Manyame |
| Mushumbi Bridge | Lower Manyame |
| Muzarabani bridge | Muzengezi |
| Chidodo | Muzengezi |

The investigated rivers consist of lateral banks and are confined by continuous natural levees. During floods, the flood plains of the rivers will be filled and the water may rise till the natural levees.

When the water level in a river is higher than the groundwater level water flows from the river into the soil and the river is considered influent. If this continues for a considerable length, the river may dry

up during rainless periods and these rivers are classified as ephemeral. Ephemeral rivers are common hydrological features in Southern Africa where periods of up to 6 months occur with no significant rainfall. These rivers are excellent to determine the geometric profile of a river, because in the dry season there is no water. For this research several measurements in these rivers were done in the month March, where the rivers still carried water, but the flood plains where dry.

## 2.2 Selection of gauge sites

Gauging stations should be located at points where the discharge changes abruptly, i.e. downstream of confluences and bifurcations, or at other places to provide data used for calibration of hydrological models. Because of the demonstration purpose of this research, not all the gauging station comply to this requirement. Gauging station Chidodo is located near the border of Mozambique, which is useful to obtain insights in the amount of water leaving Zimbabwe from one specific catchment area. Muzarabani Bridge is located just in the valley nearby the escarpment that represents the separation between the plateau and the Zambezi valley.

In order to determine a reliable rating curve, a fixed relationship between discharge and water level must be assured. A gauge, therefore, should not be placed directly upstream of a confluence or bridge, where backwater effects may spoil the relation. Therefore several gauging stations are located just after a bridge and there is sufficient distance between the gauging station and the confluence with the Zambezi river downstream to avoid backwater effects.

In alluvial rivers, reaches where degradation or aggradation of the river bed may be expected either due to accelerated or retarded flow or to regime effects, should be avoided as much as possible. Such variations of the river bed influence the water level and spoil the stage-discharge relationship. A location of a gauge in a rocky section free from backwater effects is attractive for obtaining a reliable rating curve, due to the absence of morphological effects. The gauging station at Angwa bridge is located at a rocky section.

Reasonably straight river reaches should be selected in order to avoid transverse slopes of the water surface, especially under high discharge conditions. These criteria have been taken into consideration for choosing the locations of the gauging stations, but could not always be fulfilled.

# 3 Theoretical framework

## 3.1 Traditional method of determining rating curves

The rating curve considers the discharge as a single function of the water level. The following power law function is mostly used to approximate the rating curve:

$$Q = a(h - h_0)^b \tag{1}$$

where $Q$ is the discharge [m$^3$/s], $h$ is the water level [m], $h_0$ is the water level at zero flow [m], $a$ is a coefficient [m$^{3-b}$/s) and $b$ is a coefficient [-]. The power law is a functional relationship between two quantities, where a relative change in one quantity results in a proportional relative change in the other quantity. In reality the flow capacity of a river channel and adjacent floodplains is affected by the cross-sectional geometry, the bottom slope and the type of cover of land that is directly related to flow resistance. This is captured by the Manning formula (Manning, 1891) that describes the discharge of steady uniform flows and is compatible with the power law function, but more physically based. The formula is derived based on the assumption that the frictional resistances forces are balanced by the gravitational forces.

$$Q = K\sqrt{S}AR^{2/3} \tag{2}$$

where $K$ (or $n^{-1}$) is Manning's coefficient, $S$ is the water surface slope [-] (or the gradient of the riverbed assuming uniform flow), $A$ the cross sectional area [m$^2$] and $R$ is the hydraulic radius [m], which is given as follows:

$$R = \frac{A}{P} \tag{3}$$

where $P$ is the wetted perimeter [m]. The last part in the Manning formula, $AR^{2/3}$, is also called the conveyance, which completely depends on the cross-sectional geometry.

The traditional method used to obtain $a$, $b$ and $h_0$ from formula 1, is to fit the power law function to the water level and discharge pairs measured in the field. The coefficients are determined by minimizing the Root-Mean-Square-Deviation, representing the sample standard deviation of the differences between predicted values (rating curve) and observed values.

### 3.1.1 Limitations traditional method

The main limitation is that the curve is not physically substantiated, which introduces uncertainty in the inter- and extrapolation of the rating curve and the particular form of the rating curve. In general the measurements are done during regular flow conditions, which means that a large part of the rating curve is based on extrapolation. Coefficient $b$ in the traditional rating curve formula (1) barely influences the rating curve for regular flow conditions, while the high flow conditions are very sensitive to this coefficient. This is shown in figure 2. Small errors in these measurements contribute to larger errors during flood conditions. Limited observations over a limited range may cause unreliable rating curves in the extrapolation zone, which may be reinforced by measuring errors.
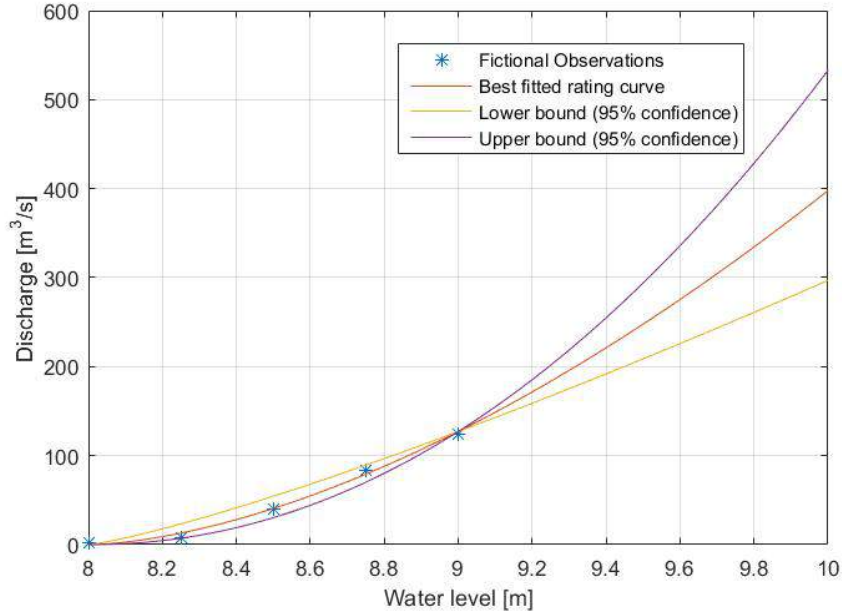
Figure 2: Sensitivity of the rating curve to exponent $b$: The 95% confidence interval shows that it mearly influence the regular flow conditions, but strongly influence the high flows.

Another limitation is the fact there could still be deviations between the rating curve and real discharge in the river, caused by cross-section changes due to vegetation growth and/or bed movement. Scour and redeposition shape the profile of the river during the year, which makes the rating curve for a limited time period valid, before it needs to be recalibrated again. This period depends on the dynamics of the river and the adjustment time relies on expert judgement. Recalibration of the rating curves are time consuming, because new discharge and water levels measurements need to be gathered containing observations pairs spread over several different flow conditions.

In practise the rating curve the coefficient $a$ is used as a "dust-bin" in the power law function, representing the roughness coefficient, water surface slope and geometry. However, a "dust-bin" also consists of physical processes that are not captured by the theory, due to errors or simplifications.

## 3.2 Physics-based Rating Curves

Another approach to compose rating curves is by using the Manning's formula. In general the Manning formula can be subdivided as follows:

$$Q = \underbrace{Ki^{1/2}}_{a_1} \underbrace{AR^{2/3}}_{a_2(h-h_0)^b} \tag{4}$$

where we introduce $a1$ and $a2$, which form together the coefficient $a$ in formula 1.

The conveyance part of the Manning's formula can be measured in the field, as a function of the water level. Relating the conveyance to $h - h_0$ would yield the conveyance-water level relation, which can be drawn-up for the entire profile. This relationship supposed to be described very well by a logarithmic function. This relation determines the exponent $b$ and $a2$ of the rating curve. How this geometric profile of the river is measured, is discussed in chapter 3.

This only leaves the coefficient $a1$ to be determined. This coefficient depends on the river slope and the channel resistance (Manning's coefficient). The first can be determined, but there are difficulties to determine the roughness coefficient in a natural channel due to bed roughness, bank irregularity, effect of vegetation, depth of water, channel slope, and perhaps other factors(Riggs, 1976). Especially

in sand-bed natural channels there is attribution of nonrigid and highly dynamic bed (Yen, 1991). No objective way of evaluating and combining these factors into one coefficient is available and it is not a directly measurable quantity in the sense that it cannot be measured using an instrument. Three common methods for estimating the Mannings coefficient are: (1) selecting $n$ from a table of typical values based on qualitative description of channel characteristics, (2) selecting it from photographs of channels displaying typical values or (3) estimating $n$ empirically using one of several equations relating hydraulic variables to the roughness (Chow, 1959).

In general the Manning's coefficient is not constant over the entire river profile. At floodplains the Manning's coefficient is in general lower (which means less conductance in the river) due to the growth of vegetation compared with the main channel. However, Chow (1959) showed that a uniform Manning's coefficient can be used for the entire river profile, because of parameter compensation, while remaining almost equivalent performance of hydraulic models. This is because the roughness will decrease with increased water levels, however if the floodplains of a river are rougher than the channel bottom (trees and brush), then this will compensate the $n$ value.

Moreover, a verified value of a roughness coefficient is affected by the inaccuracies in each of the other variables in the Manning equation. Inaccuracies may arise because of a poorly defined water surface slope or nonrepresentative cross sections. A poorly defined profile may be caused by bank irregularity at the high-water line or a changing cross-sectional area and shape throughout the reach. In the ideal situation, the roughness coefficient is included in a calibration process, where observations of the dependent variables is used to predict the roughness coefficient. If calibration is not possible, the roughness coefficient is estimated to establish the physics-based rating curve.

## 3.3  Application of rating curves in hydrological and hydrodynamic models

A Hydrological model is a simplified and abstract representation of how we perceive reality, which is often expressed in mathematical terms. It is an important tool to understand the movement and distribution of water within the hydrlogic cycle. These models allow us to predict runoff levels and amounts, predict water quality and get a better understanding of the underlying processes. Data is necessary to set-up and run a simple conceptual model (times-series of precipitation, temperature and observed stream flow) to obtain reliable results.

A hydrological model can be described in a mathematical form as follows:

$$Y \longleftarrow m(X, \theta, S_0) \tag{5}$$

where $Y$ is observable system states and outputs (also called system response), $m$ is the hydrological model, $X$ are the inputs, $\theta$ represents the model parameters and $S_0$ is the initial and boundary conditions. In a calibration process, the calculated system response needs to show sufficient high degree of similarity with the observed time-series and the calibration parameters in the model are adjusted to achieve this. Comparing the simulated and observed hydrograph is the mostly used comparison. However, the observed hydrograph has large uncertainties. Instead of calibrating on river discharge, there is a new approach for hydrological calibration on the basis of water level data only developed. This is done, because there are almost no uncertainties in water level measurements. The hydrological model is able to calibrate the coefficients $a$, $b$ and $h_0$.

With the physics-based rating curve, the calibration process can be even more reliable. The coefficient $a1$ can be included as a calibration parameters in hydrological models, while coefficients $a2$, $h_0$ and $b$ can be determined from field surveys. Calibration of hydrological models on water levels and in addition one more calibration factor.

# 4 Methodology

To determine the geometric profile of a river reach, different techniques for different parts of the profile have been used. Distinction has been made between the main channel and the riverbanks, respectively the part under and above the water level.

A photogrammetry technique is used to reconstruct a 3D surface map of the riverbanks. This technique can not be applied to the underwater river topography, therefore an Acoustic Doppler Current Profiler (ADCP) has been used, which measures the profile of a river and the discharge at one specific cross-section. The disadvantage of this technique is that a boat is needed and it is very time-consuming and costly. However, during periods when the river is dry (in the winter) the whole geometry of the river could be determined with the photogrammetry technique, which is a very accessible technique. At several locations the topography of the main channel has been estimated, because the locations were too remote and difficult to get with a car and boat. The locations where it was possible to launch the boat, we arranged it with the help of some locals and gave them a ride back to there hometown (see figure 3.)



Figure 3: Taxi ride back home after the locals helped us launching and returning the boat

Both parts of the river profile are needed to determine the relationship between the conveyance and water level. The obtained data from both techniques are merged and a terrain analysis is carried out to obtain this relationship. Due to hardly accessible places and strong currents, it was not possible to execute ADCP measurements at all the locations. Table 2 shows an overview of the executed measurements at different gauging stations.

Table 2: Overview of measured profiles at the gauging stations.

| Research stations | Topography main channel | River banks |
|---|---|---|
| Angwa Bridge | | ✓ |
| Nyambudzi School | ✓ | ✓ |
| Mushumbi Bridge | ✓ | ✓ |
| Muzarabani Bridge | | ✓ |
| Chidodo | | ✓ |

In the chapter three parts can be distinguished. First the photogrammatry technique will be described in section 4.1. The precision and applicability is evaluated and the general workflow of this technique will be elaborated. Secondly the method that is used to reconstruct the river topography will be discussed. A description of the ADCP measurements and the estimation of the river topography by lack of ADCP measurements are presented in section 4.2. As last is in section 4.3 explained how these two techniques are combined and the terrain analysis is executed.

## 4.1 3D image-based surface reconstruction

In different kind of science, high-resolution three-dimensional representation of geometric data is required. Nowadays a range of tools are available to capture these data and are dominated by active source sensors, predominantly based upon laser scanning techniques (e.g. LiDAR). These techniques measure distance to a target based on the travel time of reflected light on objects. A new technique in high-resolution 3D data collection is developed, which is widely accessible: Photogrammatry.

### 4.1.1 Stereo photogrammetry from aerial surveys

For already a long time photogrammetry is used for measurements from photographs and the main purpose was the construction of topographic maps. Photogrammetric analysis may also be applied to measure and record complex 2D and 3D geometric data. A fundamental method in photogrammetry is stereophotogrammetry, which is the technique of using two or more overlapping photographs to reconstruct the 3D coordinates of a set of given points shared in both photographs. Large areas can be recorded effectively using an aeroplane or satellite, while smaller areas can be recorded by a small UAV. Now this technique contributes to the results of imagery analysis into computational models by using digital/automated processing. With the advances in computational power and computer vision new image processing algorithms became available and collections of overlapping photographs can be automatically processed to rapidly extract the relative 3D coordinates of surface points on pixel scale.

The data that is required, consist of only digital photographs and can be obtained with any commonly available digital camera. The camera properties, like focal length and resolution, defines the quality of the 3D reconstruction. The technique facilitates rapid collection of large amounts of data in remote settings where portability and efficiency may be critical. A second advantage is photo-based 3D reconstruction techniques can provide a comparable resolution to laser scanning tools with a significant reduction in cost, infrastructure, and processing requirements.

In this research there is made us of Agisfot software. Agisfot PhotoScan is a commercial software, which is able to identify depth information by use of stereophotogrammetry. PhotoScan does not display the statistical results of the photogrammetric processing and is in science considered as a sort of "black-box" software, because there are almost none references of the detailed processing (Dall'Asta & Roncella, 2014).

### 4.1.2 Aerial photography

Aerial photography is the taking of photographs of the ground from an elevated (in the air) position. In this research a camera underneath an Unmanned Aerial Vehicles (UAV), commonly known as a drone is used for the tacking of aerial photographs. A Phantom 3 professional is used and got a built-in camera with an integrated gimbal to maximize stability of the camera in order to capture clear, stable images. The specifications of the camera are as follows:

Table 3: DJI Phantom 3 professional camera specifications.

| Camera Specifications Phantom 3 professional | |
|---|---|
| Effective pixels | 12.4 M |
| Focal length | 3.61 mm |
| Sensor size | 1/2.3" (6.17 x 4.55 mm) |

Several mobile application are available to control the drone: e.g. flight path, gimbal, camera and other aircraft functions. The standard DJI GO app offers ground station features which are limited in that they must be employed in real time during the flight. Litchi, on the other hand, allows you to pre-program missions prior to flight. This mode is called Waypoint mode, where several parameters can be assigned to entire missions (e.g. aircraft speed and rotation direction), while others can be assigned individually to waypoints (e.g. heading of aircraft and curve size). The pre-programmed missions where

applied, because of the remote gauging stations where internet connection is scarce. An example of a pre-programmed mission is shown in figure 4.
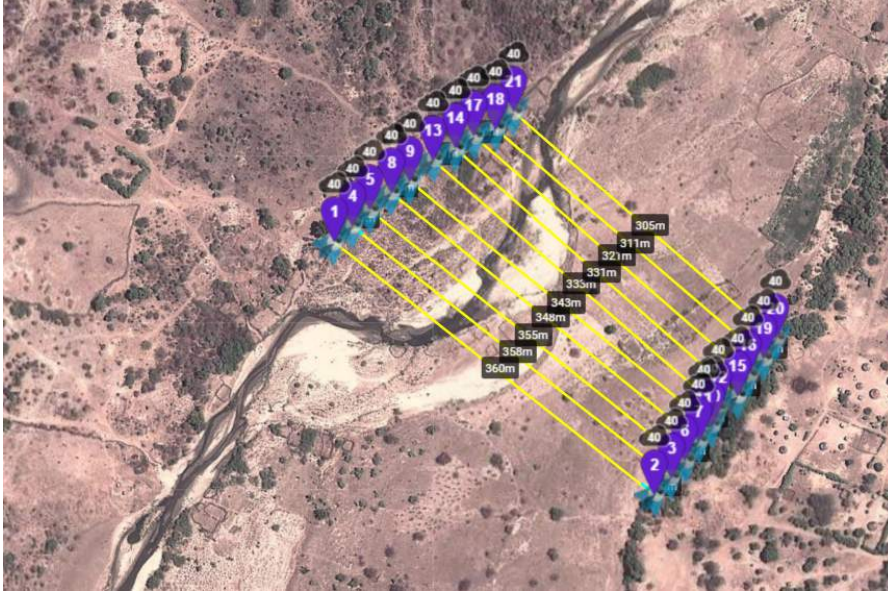


Figure 4: A flight map at the gauging station Nyambudzi School.

Selecting the flight specifications, like fly altitude and aircraft speed, are discussed in the next subsection.

### 4.1.3 Precision and applicability

In general terms, the accuracy of a photo-based model depends upon the scale and resolution of the input images, the distribution and accuracy of control data (whether ground control points, scale measurements or camera positions), the precision and distribution of matched image points, and the network geometry (Bemis et al., 2014). The network geometry includes the number of photos, how much they overlap and how convergent the views are.

Overlapping the images obtained depends on flight altitude and plane speed, and is calculated according to the equation:

$$O = \frac{k \cdot h - \dfrac{S}{p}}{k \cdot h} \tag{6}$$

where $O$ is overlapping [%], $h$ is the altitude [m], $S$ is the speed of the UAV [m/s], $P$ is the number of pictures the camera takes per second [s$^{-1}$] and $k$ is a constant that depends on the camera vertical sensor dimension [-] and can be calculated as follow:

$$k = \frac{dh}{f} \tag{7}$$

where $dh$ is the horizontal dimension of the sensor [mm] (could also be vertical dimension of the sensor, but depends on the position of the drone and the direction it flies) and $f$ is local length [mm].

The camera of our UAV has a focal length of 3.61 mm and a horizontal dimension of 6.16 mm. The speed of the UAV is set to 1.5 m/s to avoid blurred pictures and guaranty sufficient sharpness. The altitude is chosen such that it has sufficient spatial resolution, which is indicated by the Ground Sampling Distance (GSD). The GSD is the distance between two consecutive pixel centers measured on the ground. The

bigger the value of the image GSD, the lower the spatial resolution of the image and the less visible details. A higher flight altitude leads to bigger GSD values. Different flight altitudes are used for the locations in the Middle Zambezi basin, depending on the size of the area. In most of the cases there is chosen for a GSD value of approximately 1.5 cm/pixel, which corresponds in our case with an flight altitude of 35 m. However, at Manyame river there is chosen to fly at a altitude of 40 m, because of limited flight time due to battery restrictions.

The overlap requirement is best considered in terms of coverage and angular between the overlapping images. Every surface that will be processed needs to be covered by at least 2 images taken from different positions, but preferably more. Increasing angles of convergence between overlapping images will eventually prevent matching due to the surface texture appearing too dissimilar in images from different directions. While at the same time angular changes between photos can increase the accuracy of reconstructed 3D surfaces. In this research, the camera position was directed orthogonal to the surface to reduce complexities in data collection. The overlapping percentage is set to 80% of forward overlap and 60% of side overlap ("Agisoft PhotoScan User Manual", 2017).

Now the to number of pictures that the camera takes per second can determined, which is 0.1256 per second. This is equal to an interval time of 8 seconds between two subsequently taken pictures. At the same time the flight path needs to be established in such a way that there is 60 % of side overlap.

### 4.1.4 General workflow

In figure 5, the general processing steps can be seen, which considers the data collection (fieldwork) and data processing (in Photoscan). The whole process will be discussed in this subsection
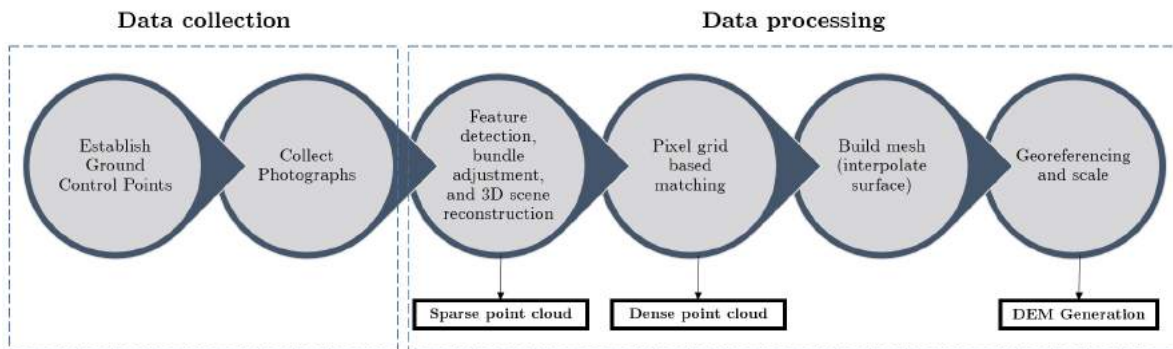


Figure 5: General workflow illustrating the reconstruction process for photo-based 3D elevation maps. Squared boxes indicate potential output products at different stages during reconstruction.

**Data collection**
The results of traditional photogrammetry are generally derived by providing additional control data. These are control points within images whose positions are known that needs to be added in the area prior to collecting the photographs, so called ground control points (GCPs). These points have three functions: 1) it allows the reconstructed scene to be placed in the real world, assigning the correct world coordinates and orientation, 2) it improves accuracies by refining parameters and simultaneously optimizes the variables, with minimized overall error and 3) it allows error estimates. Compact discs (CDs) are placed in the area and surveyed using the theodolites. The GCPs are distributed widely across the reconstructed surface area and it is recommanded to place atleast 10 of them. However, greater accuracy is achieved with more GCPs. By simply knowing the coordinates of the GCPs on an input image, photoscan is able to scale the model. Another possibility of georeferencing is using the camera locations of the input images, but these are insufficient for the accuracy requirements of a DEM

generation in our case.

Other key considerations of data collection are the effects that reduce textural variability within images and changes in illumination. Common issues preventing algorithms from resolving coincident points include homogeneous surface texture, which is often due to surface reflections and flat surfaces with little textural variation. Changes in illumination may be caused by filtering by clouds.

In order to determine the 3D coordinates of locations along the river, two land surveying tools are necessary: a theodolite (including a tripod) and a surveying pole. A theodolite is a instrument that measures both horizontal and vertical angles and is used in triangulation networks and geo-location work. Together with a surveying pole the 3D coordinates of the GCP can be determined. This technique induces errors which should be minimized. Instrument misadjustments can lead to significant errors, but also errors in readings may occur. A double check for equipment installation and readings are necessary and are also applied in this research. Errors will always be there, but we tried to minimize the error to reasonable tolerance.



Figure 6: Determination of the three-dimensional coordinates of a GCP (CD underneath the pole) on a floodplain of the Manyame river downstream of the Mushumbi bridge.

**Data processing**
After the GCPs are placed, the UAV is launched and it flew the pre-programmed trajectory generated in the software programme Litchi. The detailed information about this flight and the data acquisition, like height, fly speed and capture interval, are discussed in subsection 4.1.3. Figure 4 shows the flight map of the UAV at Angwa river. After the photographs of the area where taken the data processing can start.

The first step in the data processing is so called 'Structure from motion' (SfM) method. This method detects features across the photos which are stable under viewpoint and lighting variations. There is no exact definition of a feature and their properties often depends on the problem or the type of application. A general identity property of a feature is that it is an "interesting" part of an image. SfM method generates a descriptor for each point based on its local neighborhood. With these image feature descriptors, bundle adjustment can be initialized. It uses the matching features in multiple overlapping images to establish the relative locations of each camera and scene geometry simultaneously and automatically(Westoby, Brasington, Glasser, Hambrey & Reynolds, 2012). This results in a 3D reconstruction of the matched features, which will be in an arbitrary coordinate system. This is called a sparse point cloud (or tie points), that represents the structure of the surface.

Now the georeferencing can be carried out, which means that an internal coordinate system of the sparse point cloud can be related to a ground system of geographic coordinates. The sparse point cloud can be scaled to the real world by imposing the xyz-coordinates of the GCPs.

Thirdly, a dense point cloud representation of the surface is produced. For reconstructing the dense surface there are several processing algorithms available in Photoscan. Exact, Smooth and Height-field methods are based on pair-wise depth map computation, while fast method utilizes a multi-view approach("Agisoft PhotoScan User Manual", 2017). In general it means that the algorithm will search systematically over a pixel grid to identify best matches between images, which results in significantly more 3D points. This method is more precise than the SfM method. In Agisfot there is the option to adjust the quality of the reconstruction to manage the resolution and time required to produce the dense point cloud.

A polygonal mesh model can be generated based on the dense point cloud, where there are two different type of methods available in Photoscan. In this research, the 'Height field' surface type is applied that is optimized for modelling of terrains. At the same time some surface areas within a circle of a certain radius around every dense cloud point will be interpolated. This covers some holes in missing data, but there can still be some holes present in the model, which are to be filled at the post processing step. It is also possible to edit the geometry to remove unwanted objects, for example introduced noise by water, human beings or equipment that was still in the area during the flight. Now a DEM can be created and during this process the Inverse Distance Weighting interpolation method is used to fill the remaining gaps from the dense point cloud.

The DEM can be exported according to user defined specifications. The export file consists of a regular grid of height values and is rasterized from the dense point cloud data. The size of the raster can be set manually, with the pixel size as minimum value. There is chosen for an 10 cm by 10 cm raster size, because of computational power and needed accuracy. This DEM is used in further analysis (see section 4.3).

## 4.2   Reconstructing the river bed topography

Initially, it was planned to measure the topography of the main channel at all the research stations, however, because of limitations on time and logistical constraints, the amount of bathymetry measurements was reduced to two gauging stations: Nyambudzi School and Mushumbi Bridge (see table 2). The complete river profile of those two sites could be constructed, while for the other sites the profile of the main channel is estimated based on the judgement of an observer and / or empirical relationship for channel width and depth.

Acoustic Doppler Current Profiler (ADCP) measurements is a measuring technique to determine discharges and cross-sectional areas from boats moving across river transects. This device uses acoustic pulses to measure water velocities and depths using the Doppler effect of sound waves scattered back from particles within the water column. Figure 7 shows the preparation of an ADCP measurement at Mushumbi bridge. The team secures the hydroboat with the ADCP on it safely to the left side of the boat.

Figure 7: Preparation of an ADCP measurement at Mushumbi Bridge

The accuracy of the estimated discharges and cross-sectional profiles are relatively good compared with the existing measurement alternatives. Figures 8 and 9 show cross-sectional profiles from ADCP measurements at resp. Mushumbi Bridge and Nyambudzi School. At Mushumbi bridge it can be seen that at a certain moment a break in the slope at the bottom of a stream bank occurs, where the water surface would begin to recede in a more horizontal direction from the stream banks when flows are decreasing. The channel can be considered as a riffle channels with a rectangular cross section, while at Nyambudzi School the channel is more like a trapezoidal cross section.
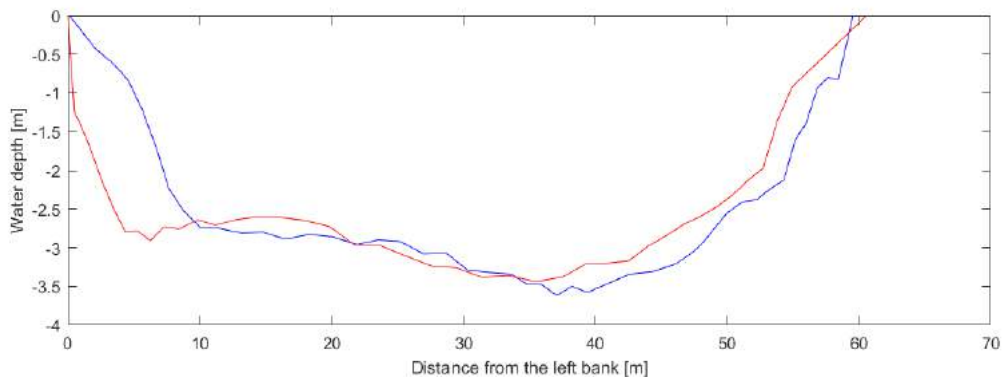


Figure 8: The cross-sectional profiles from two different ADCP measurements at Mushumbi Bridge.
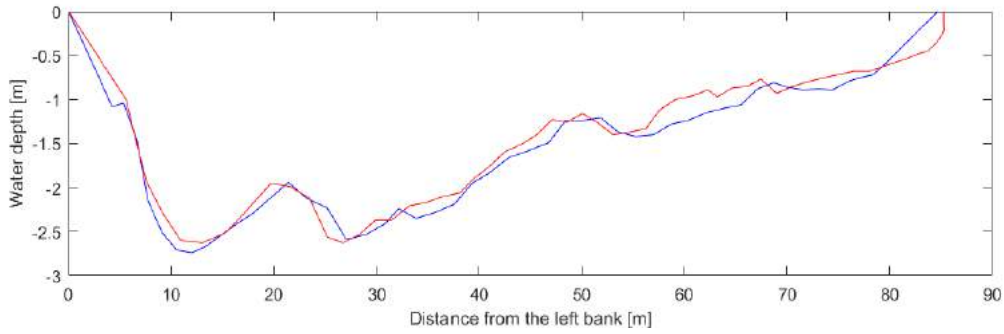
Figure 9: The cross-sectional profiles from two different ADCP measurements at Nyambudzi School.

If an ADCP measurement was not possible, the river topography of the main channel was estimated using the width-depth ratio and the information that observers at different gauging stations gave us. The width-depth ratio represents the natural angle of repose of the sediment material in still water for alluvial rivers. A theory developed by Lane (Lane, 1995), based on an equilibrium of forces acting on a particle in a channel cross-section, results in the sinusoidal shape of a stable cross-section:

$$h = \frac{2 \tan \varphi B}{\pi^2} \tag{8}$$

$$h_m = \frac{h\pi}{2} \tag{9}$$

where $h$ is the average depth, $h_m$ is the maximum water depth, $\varphi$ is the natural angle of repose and $B$ is the width of the channel. These parameters are visualized in figure 10.
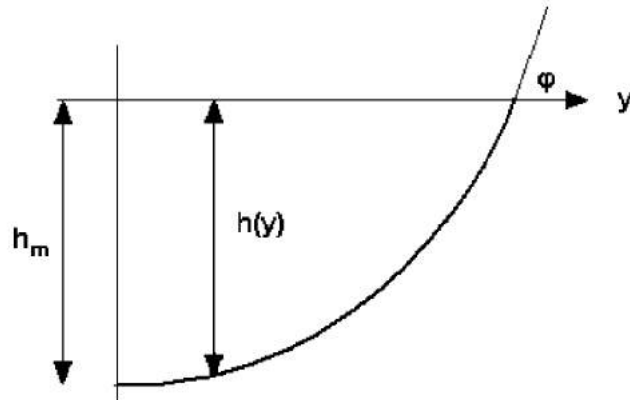


Figure 10: Visualization of different parameters in Lane's theory (Savenije, 2003)

The average width of the river as function of the elevation (of the river banks) can be determined from the 3D-surface reconstruction. The determination of these 3D-surfaces is further explained in section 4.3. Figure 11 shows the width- water level relationship for two gauging stations. Elevation and water level can be confusing, but are in this research considered as the same. Fictional water levels of a certain elevation are imposed in 3D-surface models to determine geometrical river parameters. By drawing the tangent at the lower range of the graph and the natural angle of repose can be determined by multiplying this angle by two, because of a riverbank at each side of the river.
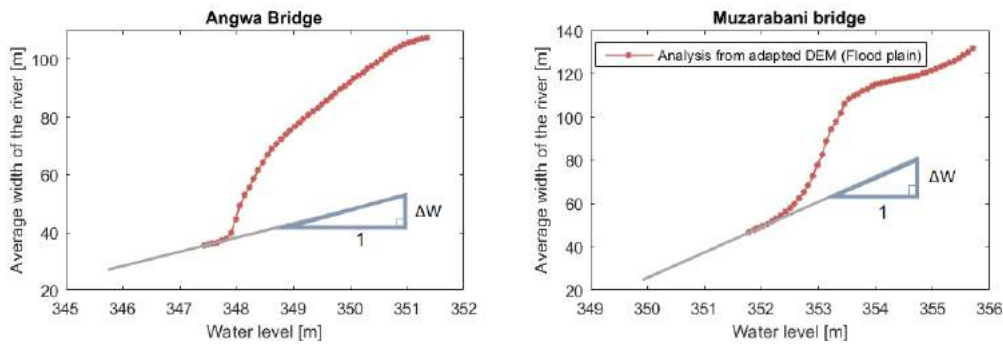
Figure 11: Relationship between width and water level and the extrapolation to lower water levels to estimate the river topography.

This information gives as the natural angle of repose and width of the river (reach-averaged values) and the average and maximum water depth can be determined, where the shape of the cross-section is a sinusoid. This method is tested for the two gauging stations at which the topography of the main channel is known. Table 4 gives the geometric information from the DEM at the gauging stations and also the known average and maximum depth from the stations where ADCP measurements where done. The results are not very reliable, because of the large deviation at the Nyambudzi school. This can be explained, because the water level at that moment was almost at bankfull level and therefore the width-depth ratio represents the floodplains in the lower range, but not the main channel.

Table 4: My caption

| | DEM | | Lacey's Formula | | ADCP/expert | | |
|---|---|---|---|---|---|---|---|
| | $\tan \varphi \ (= \dfrac{1}{\Delta W/2})$ | W | $h_m$ | h | $h_m$ | h | Absolute error (m) |
| Angwa Bridge | 1/2.00 | 35.5 | 5.47 | 3.6 | - | - | - |
| Nyambudzi School | 1/36.4 | 69.0 | 0.60 | 0.38 | 2.75 | 1.50 | 1.12 |
| Mushumbi Bridge | 1/4.81 | 61.5 | 4.08 | 2.60 | 3.50 | 2.27 | 0.33 |
| Muzarabani Bridge | 1/6.33 | 47.0 | 2.35 | 1.5 | - | - | - |
| Chidodo | 1/2.64 | 35.0 | 4.21 | 2.68 | - | - | - |

Based on the method developed by Lane and the information from the observers at the gauging stations, it is assumed that the slope of the banks continues till a certain depth and from where the riverbed is flat; a rectangular cross-section without a riffle on the riverbed. An example is given in figure 12, which gives the main channel topography at Chidodo.
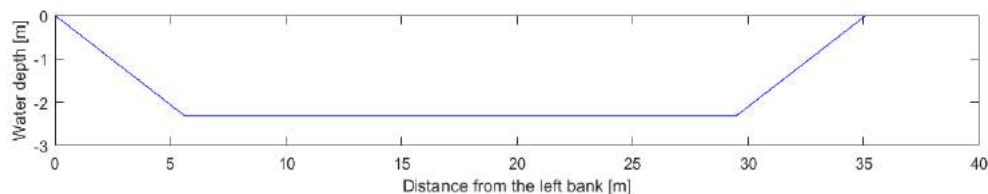


Figure 12: The estimated cross-sectional profile at gauging station Chidodo

## 4.3 Terrain analysis

After a 3D surface map is created in Photoscan, the software is able to export a digital elevation model that represents a surface model with a raster size of 10 by 10 mm. After that the data is further processed in Matlab.

The first step is to get rid of the noise in the DEM introduced by the water. The points of the dense cloud that are classified as water have been deleted and during the post processing step the

water surface area is interpolated, but this introduces errors (see figure 13; bad visualization because of maladjusted elevation scale). Interpolation occurred between the two riverbanks, but in practical terms it is unworkable to delete exactly the water points and not partly the river banks. So interpolation has been done between points that are not defining the elevation at the edge of water and riverbank (also higher grounds), which produces errors in the water surface area. Therefore we need to set the elevation of the water surface area manually at a certain level.
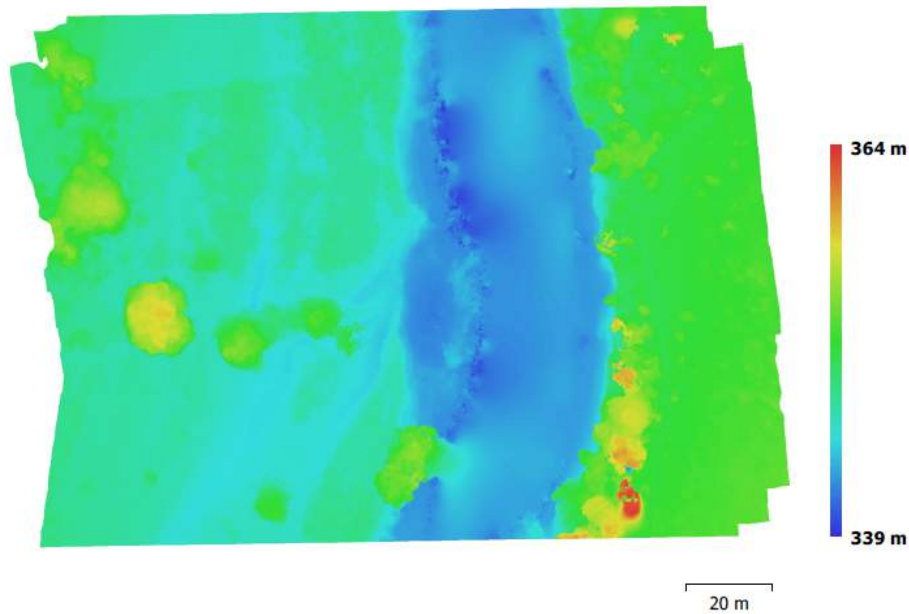


Figure 13: Reconstructed digital elevation model in Agisoft of the gauging station Chidodo. The elevation model gives a noisy area at the water surface.

After exporting the DEM from Agisoft, the elevation of the DEM-cells between the two river banks must set to an elevation that is equal to the water surface elevation in situ. So in order to do so, the xy-coordinates of the river banks need to be known and also the water surface level in situ. The latter can be done by reading the elevation of several points that lie on the waterline in Agisoft and applying the law of averages. However, to know the exact coordinates of the river banks according to the proper raster is difficult. This is why a simplification is applied, where a Fourier series is fitted through several xy-coordinates of the river banks. The xy-coordinates of the river banks are obtained by drawing a polyline along the waterline by using a orthomosaic map (right map in figure 14).
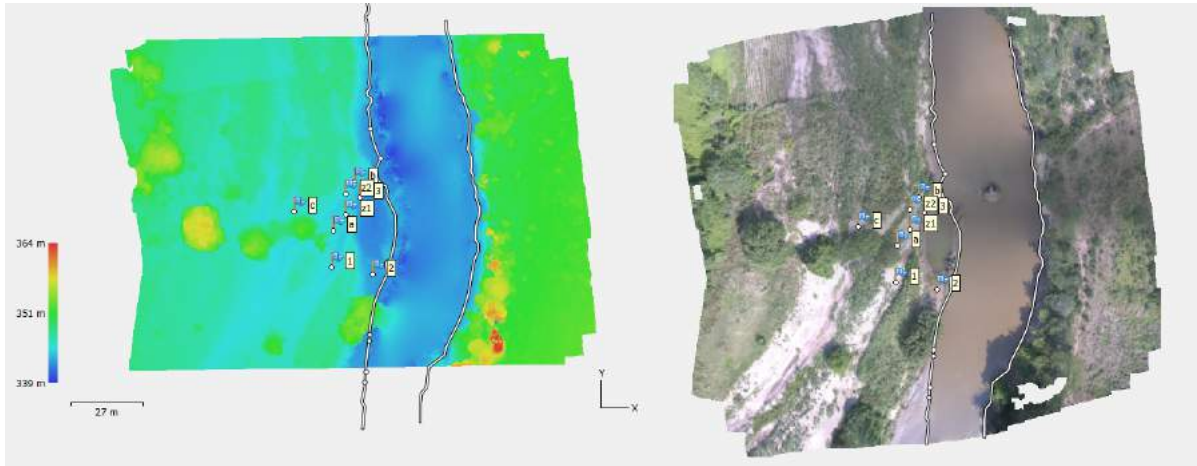
Figure 14: Right: Orthomosaic map of the gauging station Chidodo where polylines are defined that describe the riverbanks. Left: the polylines presented in the DEM.

The export of a polyline gives the xy-coordinate of the endpoints of the polyline. A Fourier series was used to have a continuous function that describes the waterline and is a sum of simple oscillating functions (sine and cosine functions):

$$y = a_0 + \sum_{j=1}^{n} a_i \cos(iwx) + b_i \sin(iwx) \tag{10}$$

where $a_0$ models a constant term in the data and is associated with the $i = 0$ cosine term, w is the fundamental frequency of the signal, n is the number of terms (harmonics) in the series ($1 \leq n \leq 8$). The goodness-of-fit statistics and judgement of plotted fourier series were used to determine the amount of terms in the fourier series. In most of the cases 8 terms were chosen. Two or in some cases four fourier series, depending on the amount of river banks at the gauging station, where fitted through the xy-coordinates of the polyline describing the bank obtained in Agisoft. These functions where used to calculate the xy-coordinates of the waterline that are proper for the chosen raster. The elevation of the approximate water surface, the area between the Fourier series, is set manually to the correct level. This adapted DEM will be used from now on and a schematization of the DEM represented as a raster is shown in figure 15. It is an $M$ x $N$ raster where every coordinate in the xy plane $(m,n)$ has got an elevation $z$.
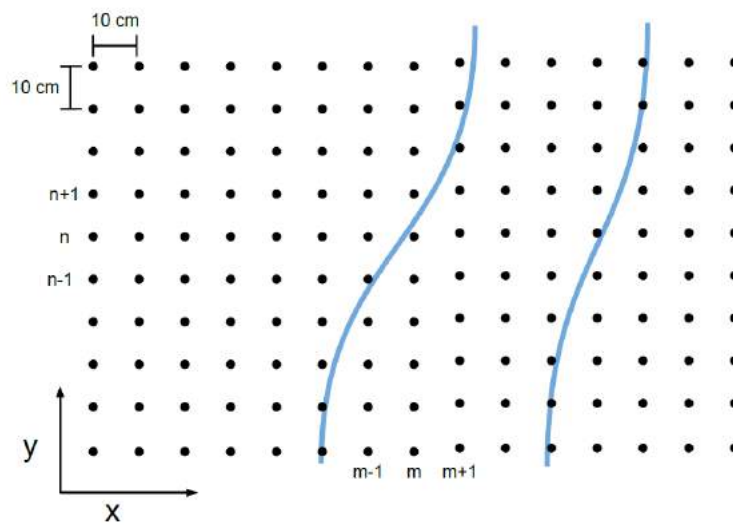


Figure 15: Schematization of the raster grid of the DEM.

The adapted DEM provides information on the geometry of the riverbank. Cross-sectional parameters can be derived from this DEM by using numerical analysis. We are interested in the following geometrical parameters: 1) cross-sectional area, 2) wetted perimeter and 3) width of the river. These parameters are functions of the water level in the river, which can be entered manually into the DEM. From now on we focus on the process in which one water level is entered. This process should be repeated for several water levels to determine the geometrical parameters for different water levels.

The cross-sectional area can be calculated by multiplying the average water depth between two adjacent measured values by the distance between those points, which is known as the trapezoidal rule. This can be done for all the cross-section in the y-direction, so that a vector of cross sections perpendicular to the flow direction can be created:

$$\vec{A} = \sum_{m=1}^{M} (x_{m,n} - x_{m-1,n}) \cdot (d_{m,n} + d_{m-1,n})/2 \tag{11}$$

where $\vec{A}$ is a vector with length $N$ consisting of cross-sectional areas, $x_{m,n}$ is the X coordinate of grid point $(m,n)$ and $d_{m,n}$ is the water depth of grid point $(m,n)$ which is computed by subtracting the elevation from the entered water level (only positive values are considered). The vector of wetted perimeters can be determined as follows:

$$\vec{P} = \sum_{m=1}^{M} \sqrt{((x_{m,n} - x_{m-1,n})^2 + (z_{m-1,n} - z_{m,n})^2)} \tag{12}$$

In this case only the elevation values are considered if the entered water level is higher than the elevation $z$: wet cells. After these calculations, the hydraulic radii can easily be determined ($\vec{R} = \vec{A}/\vec{P}$), just like the averaged values of those geometric parameters. The width of the river for different water levels can be determined by counting the amount of wet cells and multiplying by the raster size.

In general the same process is than for ADCP measurements. The only difference is that the vectors will only consist of 2 elements in case of an ADCP measurements or only one cell in case of an estimated river topography. After constructing the geometrical parameters as a function of the water level for the main channel and the riverbanks, they need to be merged to get insights of the whole river profile. This could be done be initiating start values ($A_0$ and $P_0$) for the geometric parameters of the floodplain area. After this, we have information about about the geometry of the river from bed level till flood water levels that would normally not be considered. Figure 16 shows an overview of the whole process.
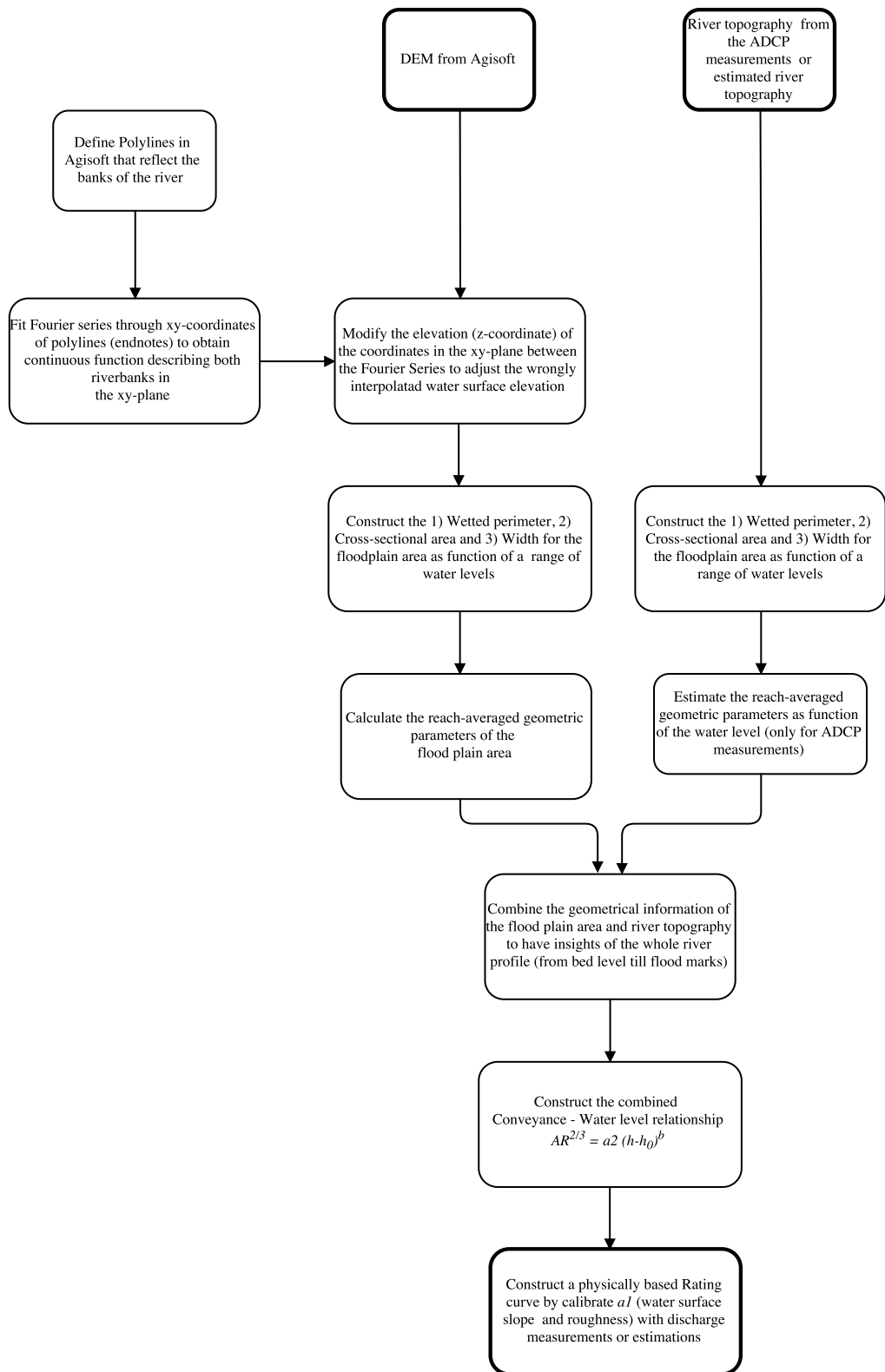
Figure 16: Flow chart of the proposed process for the terrain analysis.

# 5 Results

In this chapter the results of the terrain analysis are shown. Two gauging stations will be elaborated, namely Mushumbi Bridge and Angwa Bridge. The result of other gauging stations can be found in the Appendix C and D. These two gauaging station where chosen because of two reasons: interesting geometry and the available geometrical information. At Mushumbi Bridge, both measuring techniques where used and the whole geometric profile can be constructed. The coefficient $a1$ (representing roughness and water surface slope) could also be calibrated, because of a discharge observation. At Angwa Bridge only the river banks were measured and topography of the main channel is estimated. This research tried to predict the roughness to establish the physics-based rating curve.

In the first section the digital elevation maps will be evaluated, which is the basis of further analysis. Then two analysis on the cross-sectional river profile along a river reach are considered. The result of these analysis is the relationship between the conveyance and the water level. As last the physics-based rating curve is established and evaluated.

## 5.1 Digital Elevation Map of the floodplains of a river reach

After some modifications, described in the previous chapter, a Digital Elevation Map of a river reach is created that facilitates accurate geometric profile reconstruction. The lengths of the river reaches vary between 83 and 161 metre, see table 5 for all the dimensions of the DEMs.

Table 5: Dimensions of the DEMs at the gauging stations.

| Gauging Station | Length [m] | Width [m] |
|---|---|---|
| Angwa Bridge | 125 | 210 |
| Nyambudzi School | 110 | 423 |
| Mushumbi Bridge | 161 | 138 |
| Muzarabani Bridge | 83 | 228 |
| Chidodo | 125 | 180 |

The DEMs are the fundamental bases for analysis on the geometry of the river reaches. Figure 17 shows the DEMs of Angwa bridge and Mushumbi bridge and it can be seen that Angwa bridge has got a large floodplain at the right site of the river, while Mushumbi bridge has got a relatively small floodplain at the right side. The influence of these parts of the river are not always considered in the traditional method of constructing rating curves, because those parts only count if the observations are also done during high flow circumstances. In the majority of the cases this is not done and the rating curve, based on observations during normal flow conditions, is extrapolated to the flood conditions. However, the geometry of the river will influence the flow and the discharge related to those water levels and could significantly deviate from the geometry under normal flow conditions.
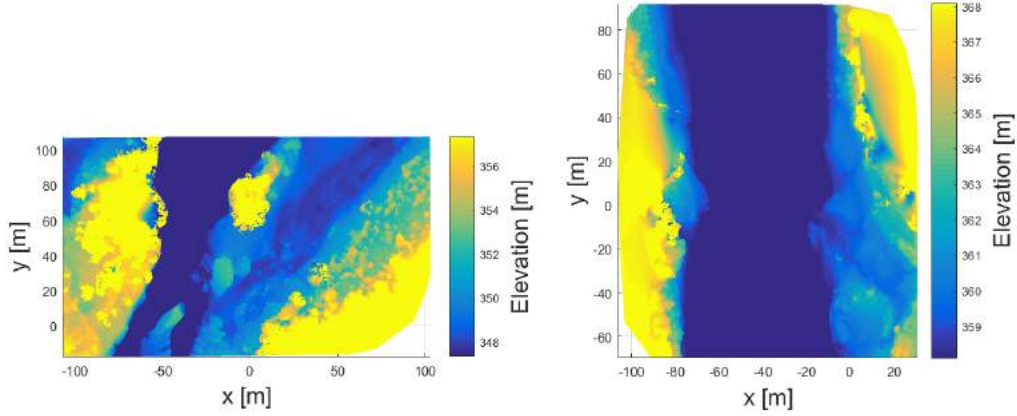
Figure 17: Digital Elevation Maps of two river reaches at the gauging stations Angwa Bridge (left) and Mushumbi Bridge (right).

### 5.1.1 Accuracy of the DEM's

Assessment of DEM quality is commonly done by a Root Mean Square Error (RMSE) value. This RMSE value is based on the difference between the reconstructed DEM 3D coordinates and 3D coordinates of Ground Control Points measured during the field survey. The total RMSE can be calculated as follows:

$$RMSE_{total} = \sqrt{\sum_{i=1}^{n}[(X_{i,est} - X_{i,in})^2 + (Y_{i,est} - Y_{i,in})^2 + (Z_{i,est} - Z_{i,in})^2]/n)} \tag{13}$$

where $X_{i,in}$ is the input value for X coordinate of the i-th GCP,

$X_{i,est}$ is the estimated value for X coordinate of the i-th GCP,

$Y_{i,in}$ is the input value for Y coordinate of the i-th GCP,

$Y_{i,est}$ is the estimated value for Y coordinate of the i-th GCP,

$Z_{i,in}$ is the input value for Z coordinate of the i-th GCP,

$Z_{i,est}$ is the estimated value for Z coordinate of the i-th GCP,

$n$ is the amount of Ground Control Points

The RMSE for other coordinate axis or planes can be calculated with the some principle, but excluding a dimension. For example, the RMSE for the XY plane can be determined by:

$$RMSE_{XY} = \sqrt{\sum_{i=1}^{n}[(X_{i,est} - X_{i,in})^2 + (Y_{i,est} - Y_{i,in})^2]/n)} \tag{14}$$

A summary of all errors is shown in table 6. On average the order of magnitude of the error is decimetres in the horizontal plane and centimetres in the vertical axis. An exception is the DEM of Nyambudzi School. The suspected cause of this large error is wrongly measured coordinates of the GCPs.

Table 6: RMSE of the X and Y coordinates, Z coordinates and total (XYZ coordinates).

| Gauging Station | $RMSE_{XY}$ [cm] | $RMSE_Z$ [cm] | | $RMSE_{total}$ [cm] |
|---|---|---|---|---|
| Angwa Bridge | 7.0 | 1.0 | | 11.2 |
| Nyambudzi School | 313.9 | 16.2 | | 314.3 |
| Mushumbi Bridge | 11.6 | 1.0 | | 11.7 |
| Muzarabani Bridge | 25.0 | 1.67 | | 25.1 |
| Chidodo | 10.0 | 2.3 | | 10.3 |

The build-up of the errors can be seen in Appendix B. Maps containing the GCPs are shown, where with colors and length scales the size of the error is displayed. There are also tables where the local errors of all the GCPs are shown.

## 5.2 Reach-averaged geometric parameters

In this section results of geometrical analysis are shown and the final result is the conveyance- water level relationship, which is fundamental for the physics-based rating curve (elaborated in the last section of this chapter). This relationship is based on observations and the power law function is fitted through the observations to obtain a continuous function of it.

The upper left graph in figure 18 shows that there is not a perfect smooth transition of the wetted perimeter between the topography of the main channel and river banks(called river resp. topography floodplain in the graph) at Mushumbi Bridge. This is due to two reasons: 1) the ADCP measurement has got some troubles with the edges of the river where extrapolation should be carried out (estimation of the shape near the river banks) and 2) the geometrical parameters are averaged over two measurements (ADCP measurement), which could deviate from the average over a reach (analysis from adapted DEM). The transition at Angwa bridge is smoothly, because the river topography is designed manually and adapted to the width-water level relationship in the floodplain area.

The wetted perimeter behaves like expected knowing that the profile is some sort of parabolic function, but with an relatively flat bed (figure 8). The point of maximum curvature in this relation corresponds to the break in slope at the bottom of the river bank where the water surface would begin to rise up in a more vertical direction from the river banks when water levels are increasing. In these cases, water levels that rise above the bottom of the bank cause smaller rates of increase in wetted perimeter for each unit increase of water level. The cross-sectional area is an continuous increasing line, which indicates that the river is becoming wider when the water levels are increasing. The combination of the wetted perimeter and cross-sectional area results into the hydraulic radius, which is shown at the bottom left corner of figure 18.
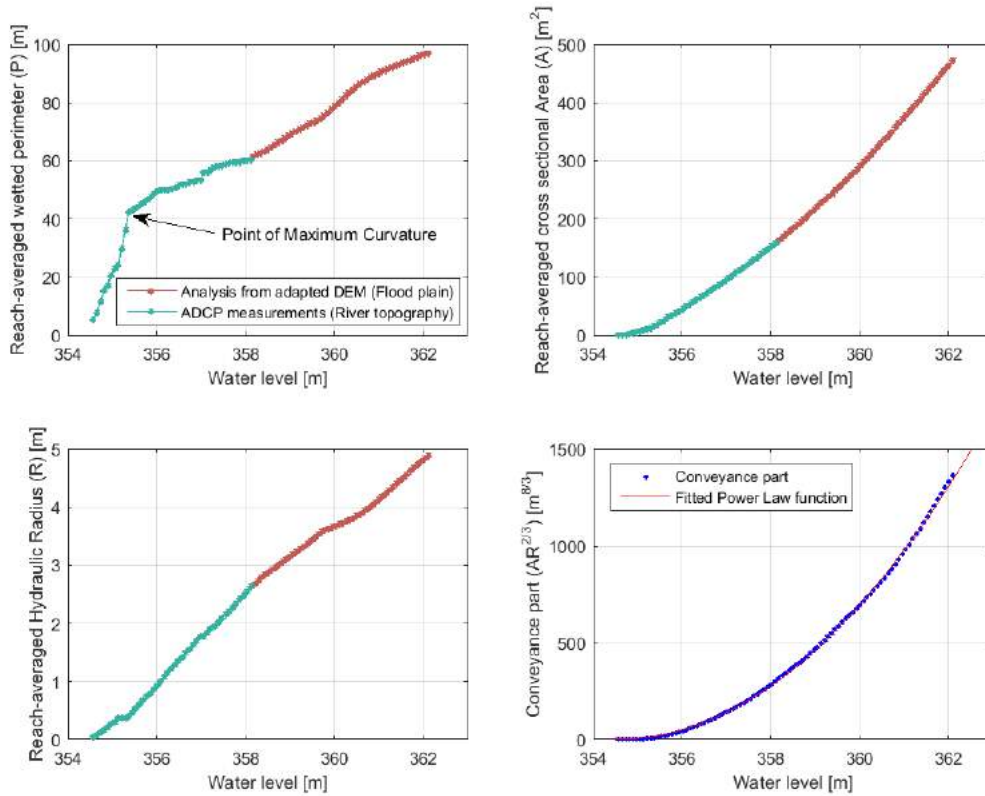
Figure 18: Cross-sectional parameters at Mushumbi Bridge, where an ADCP measurement was done for the river topography. Left upper corner: Wetted perimter - water level relationship. Left lower corner: Hydraulic Radius - water level relationship. Right upper corner: Cross sectional area - water level relationship. Right lower corner: Conveyance- water level relationship.

The conveyance- water level relationship at Mushumbi Bridge can be seen in the lower right graph in figure 19 and the power law function ($f(h) = a2(h - h_0)^b$ from formula 4) is fitted through the observations. The parameters $a2$ and $b$ were the unknowns and $h_0$ is the lowest point in the river calculated from the ADCP measurement. Curve fiting has led to the following result:

$$AR^{2/3} = f(h) = 21.28 * (h - 354.48)^{2.04} \tag{15}$$

In this case, one function describes the conveyance- water level relationship very well for the whole range of water levels. The line of best fit gives a value 2.04 for the coefficient $b$ and the 95% confidence limits are [2.026 2.054], which describes the points at a distance of twice the standard deviation of the mean from the power law function.

Figure 19 shows the geometrical information of the gauging station at Angwa Bridge, which really differs from Mushumbi bridge. The big difference is the position of the point of maximum curvature in the relationship between the wetted perimeter and the water level (top left graph in figure 19). There is no kink in the estimated river topography, because we designed a rectangular profile without ripples in the riverbed. This curvature is in the opposite direction, which means that water levels that rise above a certain point cause larger rates of increase in the wetted perimeter for each unit increase of water level. This is caused by a sudden widening of the river, suggesting a floodplain along the river. By analysing the area by means of the DEM, a floodplain at the right side of the river is noticed, which is visible in figure 20. The color limits of the map are adjusted to see the floodplain clearly.

This floodplain has an indirect effect on the conveyance- water level relationship, which makes is it hard to capture the relationship by one function (lower right graph).
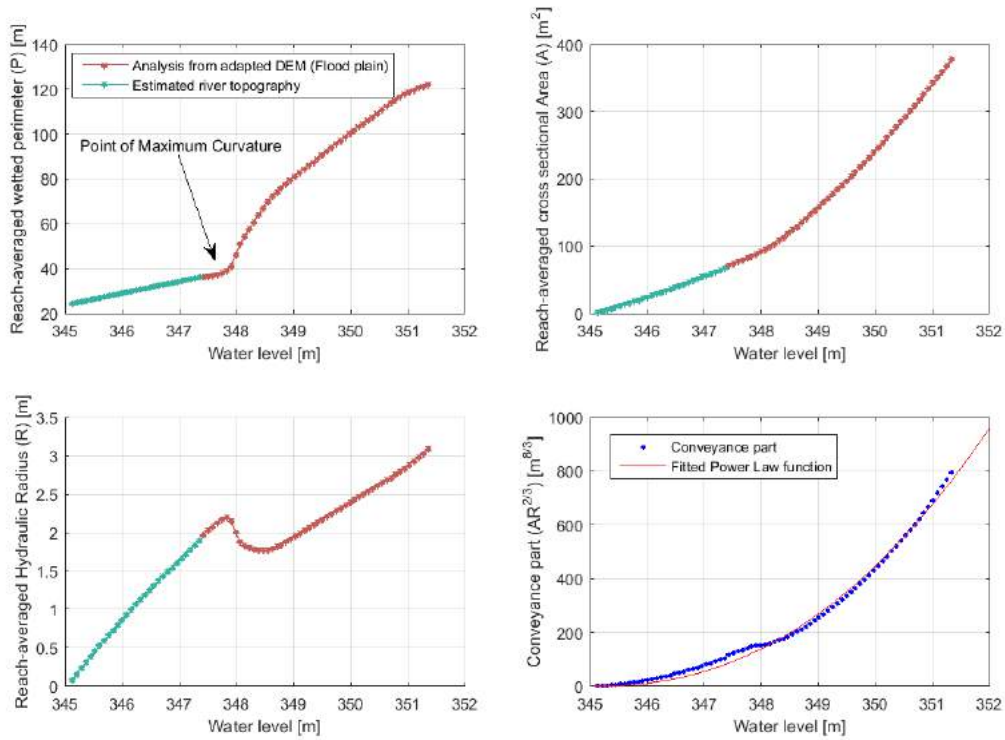
Figure 19: Cross-sectional parameters at Angwa Bridge, where the river topography is estimated (described in section 4.2). Left upper corner: Wetted perimter - water level relationship. Left lower corner: Hydraulic Radius - water level relationship. Right upper corner: Cross sectional area - water level relationship. Right lower corner: Conveyance- water level relationship.
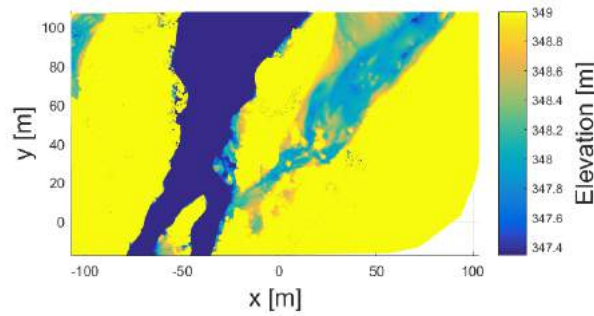


Figure 20: Floodplain at the right side of the river.

The fitted power law function is not doing well, because of the flat spot around the water level of 348 metre. To describe the conveyance part of river correctly over the whole range of water levels, there is made a distinction between the main channel and floodplains, where the mentioned water level acts as a dividing vertical line between those two areas (see figure 21). The following power law function is applied for the main channel:

$$AR^{2/3}_{main} = f(h) = 23.65 * (h - 345.05)^{1.804} \tag{16}$$

The power law function of the floodplains needs to be modified to capture the shift adjustments on water levels. This vertical shift is done by adding a constant to every $AR^{2/3}$ while leaving the x-coordinate unchanged. The minimum value of $AR^{2/3}$ in the floodplain area is used and $h_0$ is also modified to the lowest water level that belongs to the minimum value of $AR^{2/3}$. By doing this, the initial values for the

conveyance- water level relationship for the floodplain area are set correctly and the following formula is obtained:

$$AR^{2/3}_{floodplain} = f(h) = 74.16 * (h - 347.8)^{1.74} + 148.9 \tag{17}$$

It can be seen that the coefficient $b$ does not deviate significantly between the main channel and floodplains, but if we compare it with the coefficient $b$ applied for the whole range of water levels (lower right graph in figure 19) there is a deviation. The coefficient $b$ for the whole range is 2.25, which is a rather large difference considering the sensitivity of this coefficient (see figure 2 in chapter 3). This is compensated by the coefficient $a2$ and ensures that the functions are close to each other in the range of expected water levels. In this new approach, the whole range of expected water levels is considered, but this will introduce troubles in the extrapolation zone for the traditional approach.
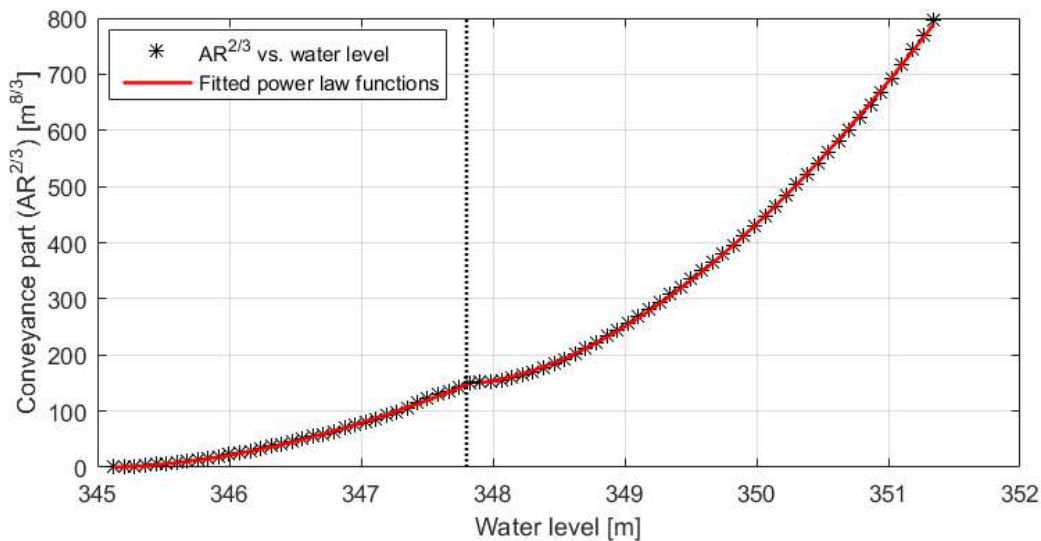


Figure 21: Fitted power law functions for the main channel and floodplains. The dotted grey line shows the water level where the two functions are separated.

Complex geometries in natural channels make the application of the Manning's formula difficult. The lower left graph in figure 19 shows the variation of the hydraulic radius as function of the water level elevation. In this case the hydraulic radius $R$ does not satisfy the condition of unique dependence on the water level elevation, which is caused by an irregular cross-section. The value of the calculated hydraulic radius is lower at higher levels than at lower levels, which is caused by the suddenly increase of the wetted perimeter around the water level 348 metre. If the hydraulic radius is not a monotonically increasing function, which is caused by the presence of floodplains, the cross-section should be divided in such a way as to separate the main channel and the floodplains. This is not executed in this research.

## 5.3   Cross-sectional changes along a river reach

The assumption of the Manning's formula is that there is a steady and uniform flow in the river. Steady indicates that the flow velocity does not change with respect to time at a given location. The flow in rivers is generally variable in time, it is unsteady, but for some practical applications the variation may be considered so slow that a steady (or quasi-steady) flow situation can be assumed.

Uniform flow refers to the hydraulic condition in which the discharge and cross-sectional area (and therefore velocity) are constant throughout the length of a channel. Considering the spatial distribution of flow in rivers, the direction and magnitude of the flow vary from one point to another. This is caused by cross-section changes along a river reach, like flow area, wetted perimeter and hydraulic radius, which make open-channel flow analysis complex. Therefore a measurement of one-cross section

may not be representative for the river.

Changes in the conveyance part of a channel were determined by comparing geometries throughout the length of the river reach. Figures 22 and 23 shows the variation of the conveyance- water level relationship of the floodplains at Mushumbi Bridge and Angwa Bridge. At Mushumbi bridge two measurements of the river topography where executed and nothing can be said about the changes throughout the length of the river reach based on two measurements.

The figures below show the range of cross-sectional changes along a river reach in which the average and the confidence belt of 95 % lie. There is a large difference between the two gauging stations, where at Mushumbi bridge the river profile is relatively unchanged throughout the length of the river in contrast to Angwa Bridge. One could say that the channel at Angwa Bridge is less uniform compared with Mushumbi bridge, which is mainly cased by the large floodplain at the right side (see figure 20 in the previous section).
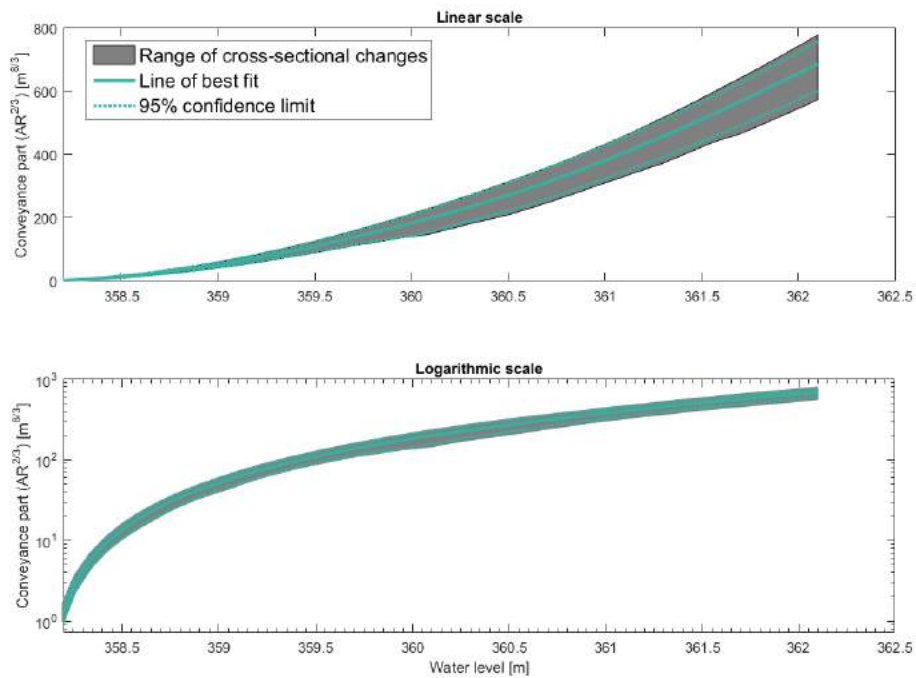


Figure 22: Cross-sectional changes along the river reach at Mushumbi Bridge. The upper graph shows the geometric changes on linear scale and the lower graph shows it on logarithmic scale.
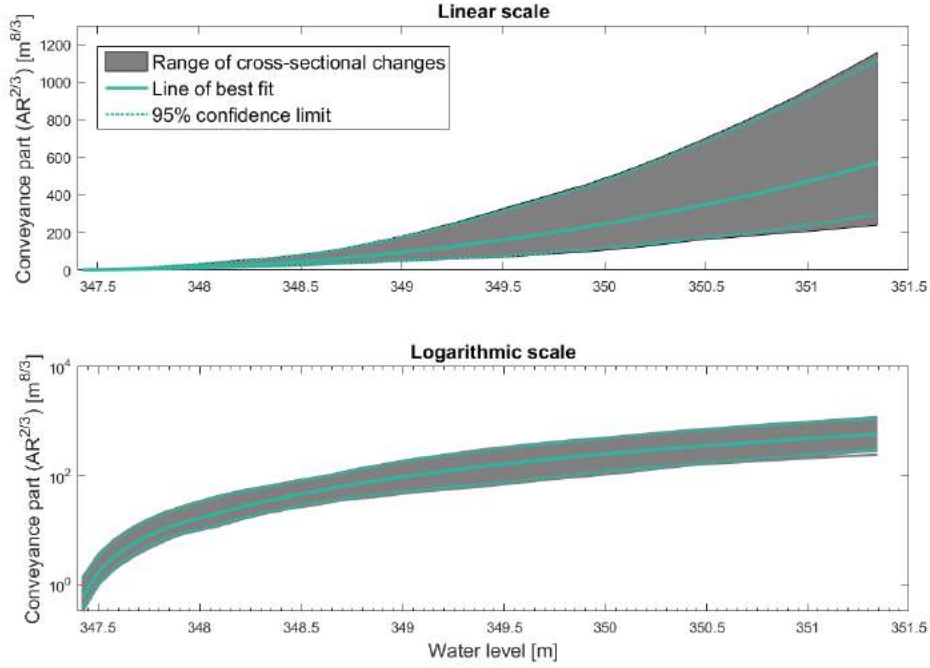
Figure 23: Cross-sectional changes along the river reach at Angwa Bridge. The upper graph shows the geometric changes on linear scale and the lower graph shows it on logarithmic scale.

In this reserach, only reach-averaged values are considered that will provide a quasi-uniform flow assumption, because local invariabilities (causing accelerations and deceleration in space) are flattened out and the river geometry is averaged over a larger length scale than one cross-section.

## 5.4 Rating curves

This section shows the final result: a physics-based rating curve. To refresh your memory, the starting point of this rating curve is the Manning's formula, where in the ideal situation the combination of two parameters are calibrated by measurements.

$$Q = \underbrace{Ki^{1/2}}_{a_1} \underbrace{AR^{2/3}}_{a_2(h-h_0)^b} \tag{18}$$

The conveyance-water level relationship (estimated by the power law function $a_2(h-h_0)^b$) is elaborated in the previous section and now the roughness and water surface slope ($a1$) needs to be determined by calibration or estimations.

### 5.4.1 Physics-based rating curves by calibration

First the approach of constructing the physics-based rating curve by calibration will be discussed. For this approach at least one discharge measurement needs to be done, which is the case for Mushumbi Bridge. An ADCP measurement includes the discharge and the cross-sectional profile, which means there is a pair of discharge and associated conveyance of the river. This pair can be used to determine $a1$ in formula 18, which is the last unknown parameter. As said before, it is valid to assume that the Manning's coefficient is constant for the whole river profile. So an relationship between water level and discharge is established based in the geometry of the river and one discharge measurement. See figure 24 for the physics-based rating curve derived by calibration. This graph includes several lines to show all the elements from the physcis-based rating curve clearly.
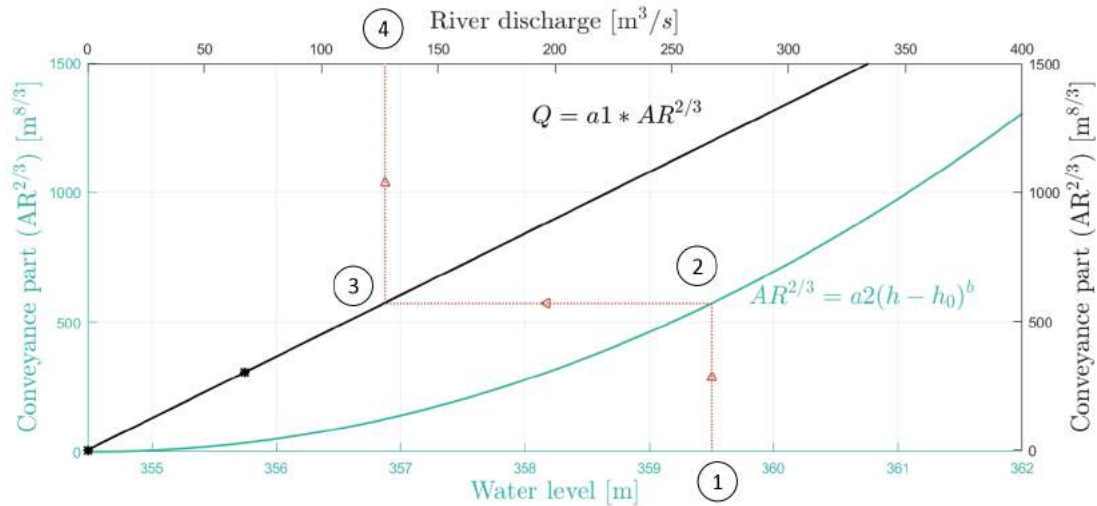
Figure 24: Physics-based rating curve at Mushumbi bridge, where $K\sqrt{S}$ (or $a1$) $= 0.2228$ m$^{1/3}$/s

On the lower x-axis, the water level is displayed and the conveyance part is displayed on the y-axis (green/blue colour). So for a given water level the conveyance part can be read from the green/blue coloured curve. There is also a secondary x-axis at the top for the discharge in the river in [m$^3$/s]. The conveyance part as function of the water level needs needs to be transformed with a linear line to the corresponding discharge (transforming with a linear line is equivalent to multiplying with a constant in a formula). The equation of this line can be derived by knowing two points on the. One observation pair is known and the line should go also go through the point (0,0) of the discharge- conveyance relation. With these two points, the black line can be constructed. The red dotted line shows the roadmap of this graph with the following steps:

1. First an observer needs to read the water level at the gauging station. This should by done several times a day to have insights about the response of the hydrological system.

2. If the water level at the gauging station is known the associated conveyance can be read, which is determined in section 5.2.

3. Now the conveyance part needs to be transformed by a line to the corresponding Discharge. Therefore you need to move in horizontal direction (in this case to the left, but it could be to the right, depending on the coefficient $a1$) to the point where you will intersect with the black line.

4. From this intersection point you need to move in the vertical direction towards th upper x-axis where you can read the Discharge corresponding to the water level that is read by the observer.

### 5.4.2 Rating curve based on slope-area method

At several gauging stations, no discharge measurement could be done, which means that the coefficient $a1$ could not be calibrated, but should be approached by estimates. Application of this approach, which is much less accurate than the other method described, should only be considered as an ad hoc method if the other method is not feasible.

The water surface slope is measured at several gauging stations by measuring the surface fall over a river reach. The length of those river reaches were limited by visibility and the order of magnitude is hundred metre. For example: at Angwa bridge we measured the elevation of the water near the riverbanks at two locations, which are located 258 metre apart and the measured height difference is 90 centimetres. Assuming there is no lateral water surface slope, the water surface slope will be $3.5 \ 10^{-3}$. The accuracy of this method over this length is doubtful, especially at the gauging stations Angwa,

where it is shown that the cross-sectional area along this reach is definitely non-uniform.

After measuring the water surface slope ($S = 3 \cdot 10^{-3}$) the only thing that left is the estimation of the bed roughness. This parameter is not directly measurable and could only be selected from tables (Chow, 1959) or pictures (Benson & Dalrymple, 1967). It is difficult to assign one particular value to the roughness, therefore it is chosen to do an estimate with an upper- and lower bound. The best estimate for $K$ is 35 with bounds of 20 and 50. The final result is shown in figure 25.
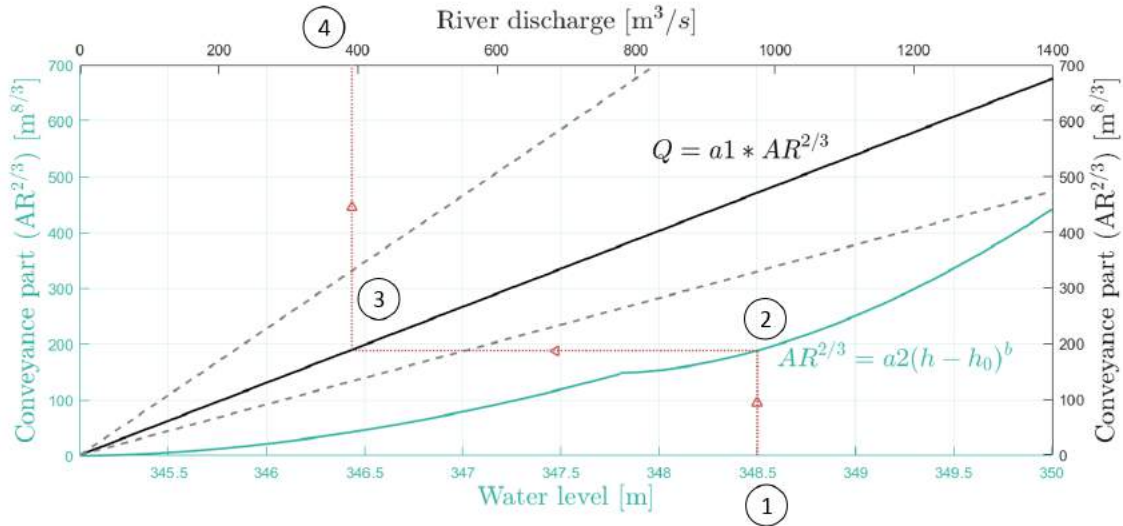


Figure 25: Physics-based rating curve, with the conveyance- water level relationship is divided into two parts as described in section 5.2. The black line is the coefficient $a1$ with roughness coefficient of $K=35$ [$\text{m}^{1/3}/\text{s}$] and the grey dashed lines are the bounds with roughness $K=50$ [$\text{m}^{1/3}/\text{s}$] and $K=20$ [$\text{m}^{1/3}/\text{s}$]

This graph also shows that the error in determination of discharge becomes larger for higher discharges. This is because of the multiplicative application of the coefficient $a1$ in formula 18. Without calibration of the roughness, the uncertainty in the rating curve can be considered significant.

# 6  Discussion

The goal of this chapter is to identify the strengths and especially the weaknesses of the method described in this report. This is done by making distinction between two different parts: 1) deficiencies and uncertainties in the process of reconstructing a 3D image-based surface model by the use of stereophotogrammetry and the combination with the topography of the main channel and 2) the application of the Manning's formula as basis of the physics-based rating curve.

## 6.1  Deficiencies and shortcomings in the determination of the river profile

A way point trajectory was set up to take pictures during a flight with a drone, which is instrumental to control the flight-settings in order to have sufficient precision for further processing. The application Litchi functioned well and makes the conduct of a flight very easy. However, there are a few concerns about GCPs that need to be placed in the area if interest. These GCPs are essential for further processing and need to be distributed widely and in the ideal situation there is a GCP visible at every taken picture during a flight.

Compact Disks, functioned as GCPs, were surveyed with a theodolite. This equipment is sensitive to human errors and may also have some instrument misadjustments. These GCP are used to georeference the 3D surface model, where the error is quantified by Root Mean Squared Errors of all the GCP in the area. An overview of the total errors at different gauging stations can be seen in table 6. The discussion about the sources of these errors is rather difficult. On one hand it shows the errors of the 3D surface reconstruction (errors in Agisoft software), but on the other it could also show the error of measuring the GCP. One out of five 3D surface reconstructions showed a significant error, while the others were accurate within several centimetres. Errors in measurements can be reduced by double checking the readings.

The reconstruction of the 3D surface model is based on the pixels in the pictures that are taken. The largest part of the river banks consists of sand or rocks, in which the surface is visible and the elevation of the ground can be determined easily. However, vegetation on the river banks will influence the 3D surface model, because the pixels in the photo will be part of the vegetation and not the underlying ground. It is expected that the vegetation will not influence the conveyance-water level relationship significantly, because bushes and trees are small compared with a whole cross-section. In this research most of the trees and bushes remained in the DEM, except for some large ones. These objects are deleted from the dense point cloud and a interpolation technique filled up those empty areas.

Stereophotogrammatry is not able to reconstruct the water surface, because of the non-stationary surface. Therefore the points classified as water had to be removed and an interpolation technique was used to fill these areas in Agisoft. However, the constructed area that is created by interpolation also consisted of unreal elevation levels, showed in section 4.3. Fourier series, acts as river banks, are used to define the water surface area, which is set manually to the water level in situ. This was difficult to determine, because you need to read the height of the pixel which is just at the edge between land and water. To reduce uncertainties, an average of several points, which are placed along the river, is taken to calculate the water level in situ. However, this might give rise to errors in the conveyance- water level relationship, because it is the transition between the 3D surface model and the river topography (measured with the ADCP). The approximate water level in situ could could slightly differ from the real one as well as the river profile.

In this research, ADCP measurements are carried out for two reasons: 1) reconstruction of the submerged river profile and 2) to have observations to calibrate the roughness coefficient and water slope. The ADCP has been used for two gauging stations, where the river is crossed over multiple times to perform a measurement. In total we crossed over the river approximately 10 times at each location, but in the end only two measurements the gauging stations were usable. This induces some uncertainties, because the two measurements deviated from each other and the average of the two has been used. Analysis of the geometry of the main channel (the cross-sectional area under water) could not be executed.

## 6.2 The use of the Manning's formula as basis of a physics-based rating curve

It is an improvement to substantiate the coefficients in the rating curves based on physical properties. The largest and most important part of the rating curve, namely the conveyance, can be drawn up for the whole range of water levels. The coefficient $a1$ still needs to be estimated and will also consists of extrapolation uncertainties, but the overall uncertainty is decreased. If the calibration technique is applied to determine the coefficient $a1$, the physics-based approach still remains with a "dust-bin" parameter, which could also be helpful to capture uncertainties and limitations of the Manning's equation: a calibration parameter may not only represent physical processes but also compensate for errors or simplifications in the equations.

Estimating the roughness coefficient, without calibration, is rather difficult and induces a lot of uncertainties. It has been shown that these uncertainties count more at higher discharges, because of their multiplicative effect. At this moment it is also assumed that the coefficient $a1$ is constant for the whole range of water levels. This may not be a valid assumption and the morphological behaviour at discharges during floods is one the main sources of uncertainties in the hydrodynamics of rivers.

One single Manning's formula for a the whole cross-sectional area of a river may induce errors. If floodplains will play a role in the cross-section, one single Manning's formula is not valid. Complex geometrical rivers make the application of the Manning's formula difficult and the river needs to divided into several parts. This is a limitation of this research, because it is not included.

### 6.2.1 The limited story of an average value

There are always effects of non-uniformities in river. In this research the geometry of a river reach was transformed to reach-averaged values in order to limit the effect of local invariabilities and non-uniformity of the river and it also sorts a lot of data into concrete and accessible information. However, this simplification will vanish a lot of information and it will not only reveal the reality but also replaces it. In figure 26 the cross sectional changes are further analysed and the reach-averaged values are split into four quarters. It is clearly visible that dividing the reach into four smaller reaches will give is rather different conveyance-water level relationships. It need to be noticed that the river reach at Angwa Bridge was less straight than other gauging stations and the river width diverged directly after the rocky part (which is after the 2nd quarter).
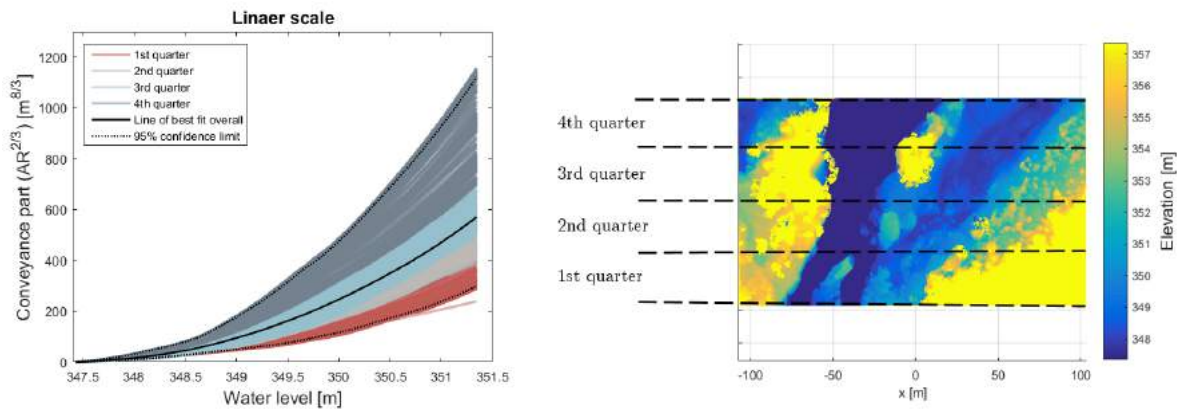


Figure 26: Cross-sectional changes along the river reach divided into four quarters at Angwa Bridge. Four quarters are defined on the right in the DEM.

During the selection of a gauge site, we tried to select a reasonably straight river. By considering a straight river it is tried to obtain a quasi-uniform reach, where local invariabilities will be vanished. In the case of Angwa bridge, the deviations of the conveyance- water level relationships along the river

reach shows a trend of widening. Given the fact that the conveyance water level relationship changes a long a reach, other physical parameters should also change in order to meet the requirement that the discharge will remain constant (quasi-steady flow) along a reach in a time interval of a few minutes (time of performing the measurement to determine geometry). According to the Manning formula the roughness of the channel (included by $K$) should increase, which means a rougher bed further downstream. At the other hand the water surface slope ($S$) should decrease further downstream. It is difficult to say which parameter has got the greatest influence in this process.

# 7 Summarizing conclusions

A new method is initiated that contributes to the aim of this report, which was the following: "Develop and evaluate a calibration method for hydrological models using a physic-based approach that captures the geometric profile of a river reach" In order to test if the above aim is achieved, first the objectives are recalled and evaluated one after another. Than the aim of this report will be discussed.

1. **Objective 1.** *Physical substantiation of exponents in the power law function, that approximate the rating curve, which depends on the shape of the river profile.*

   Instead of curve fitting through observations pairs of water level and discharge, the fundamental principles of discharge in rivers are considered. The conveyance- water level relationship is drawn up for several gauging stations in the Middle Zambezi basin. From these relationship the coefficient $b$ of the traditional rating curve could be determined as well as $h_0$. The coefficient $a$ is with this new method broken down into two parts: $a1$ and $a2$. The first coefficient represents the Manning's coefficient and water surface slope and the second one accounts for the geometry of the river (has been added because of the conveyance- water level relationship). In defining the conveyance-water level relationship the coefficient $a2$ can be determined and we end up with the coefficient $a1$. This coefficient is calibrated by an discharge/cross-section measurement or estimated. The estimation makes it rather unreliable, because the physical parametric representation of $a1$ are both rather difficult to be determined. If the water surface slope is measured over a relatively short distance (e.g. 200 metres) it is vulnerable for measurement errors. At the same time the roughness coefficient is not directly measurable quantity. The exponents that could by physical substantiated, are considered and are incorporated in the new method.

2. **Objective 2.** *Minimizing the local invariabilities that is specific to single cross-sections, by analysing river reaches, instead of one cross-section.*

   The analysis of geometrical changes along a river reach showed that the conveyance of a river changes over the length. It demonstrates that rivers have got local invariabilities causing non-uniform flows, which make in general the the open-channel flow analysis much more complex. However, the average conveyance of a reach may led to the a valid assumption of a uniform flow (which is part of the assumption in the Manning's formula), depending on the how the local variabilities behaves. In the discussion has been shown that there is a trend of widening at Angwa Bridge. Therefore other parameters in the Manning's formula also need to adjust, because the discharge is not changing along the length of the river reach. Calibration will lead to parameter compensation in the coefficient $a1$, which will also give reach-averaged results. It is shown that the location of the gauging station is important for the validity of the Manning's formula and the influence of local invariabilities at one cross-section may be decreased by using averaged value from a 3D surface model.

3. **Objective 3.** *Initiating an accessible method to calibrate rating curves, because of the limited validity due to scouring and redeposition of river profiles.*

   Calibration of this new method is much easier compared with the traditional way. Instead of collecting new discharge measurements during dispersed flows, you just have to visit the area ones with a drone and surveying equipment. It is assumed that the main reason of non-valid rating curves is cross-sectional changes. The advantage with the physics-based rating curve, the determination of discharge is divided into two parts: Conveyance part $(a2(h - h_0)^b)$ and the combination of roughness and water surface slope ($a1$). Only the 3D surface reconstruction needs to be repeated with new taken pictures to update the conveyance of the river, which can be acquired in mush shorter time. The calibration process is used to establish the relationship between coefficient $a1$ and the water level. This could be shifted because of aggregation or degradation, but the shape of this relationship will be almost unchanged.

It can be concluded that this report introduces a new calibration method for hydrological models, which is based on physical properties instead of curve fitting by an analytical relationship. This new method captures the geometric profile of a river reach and will reduce the uncertainties in the extrapolation zone of the traditional rating curve. Measurements of discharge and water levels are still important to calibrate coefficient $a1$ to reduce the uncertainties that are induced by roughness and water surface slope.

# 8  Recommendations

In this chapter two types of recommendations are given. First it is discussed how the methodology could be improved and secondly other recommendations are made, regarding e.g. the application of this method in combination with other techniques.

## 8.1  Improvement of the physics-based rating curves

In the discussion the importance of the GCP is already reported. Another relevance point about the the GCP is that you should be careful with placing GCPs underneath a bush or tree. In a DEM, each point in the xy-plane is associated with one vertical coordinate. In reality a point in the xy-plane could consists of multiple surfaces at different levels (e.g. a bridge or a tree with canopy). Placing a GCP on these locations will induce errors in the DEM generation, because it will considers solely one of those points. The dense point cloud still consist of 3D point cloud, but during DEM generation it is transformed to a 2D plane, where every point is associated with one elevation value.

It has been mentioned that there are probably measurement errors according the coordinates of the GCPs induced by the use of a theodolite. There errors consists of reading errors and misadjustment of the equipment. Another method to determine the 3D coordinates of a GCP is the use of a Differential GPS (DGPS), which will reduce the reading errors. In this research we georeferenced our 3D model to a local coordinate system. However, it is also possible to georeference it to another coordinate reference system. The advantage is that you can also use it in other GIS software, where local georeferencing could not be applied. Therefore a DGPS is much easier and transforming a local coordinate system to another is not needed.

In this research ADCP measurements were executed for two reasons: 1) the rivers were carrying water and stereophotogrammetry is not able to reconstruct the area below the water level and 2) discharge measurements are still required to estimate coefficient $a1$ of the physic-based rating curve, that represents water surface slope and roughness coefficient. The roughness coefficient is not a directly measurable quantity and errors during water surface slope measurements with the theodolite are unpreventable and should be attempted to minimize. To calculate the water surface slope within reasonable tolerance, the surface fall over the reach should be $>0.15$ m. This last criterion is defined by ISO as $\sim 10$ times the expected error of measurement of the surface fall.

In the ideal situation, the river does not carry water and you can reconstruct the river reach from bed level till the highest flood mark. However, the major setback of this approach is its necessity to execute measurements during the dry and wet season. First you need to map a river reach in order to create the conveyance water-level relationship and secondly the coefficient $a1$ needs to be calibrated by pairs of discharge and water level. In this research the largest part of the river profile was determined by using a 3D surface model, but the main channel was carrying water and the ADCP measured the profile. At the same time a discharge measurement is executed. So if you are able to visit the gauging station just ones, you should choose for the combination of 3D surface reconstruction and a ADCP measurement.

The results of the terrain analysis showed that the hydraulic radius behaves unnatural, because it was not a monotonically increasing function. In those cases, the Manning's formula needs to be modified with floodplain flow. The river needs to divided into several parts, for example the main channel and floodplain:

$$Q_{total} = Q_{channel} + Q_{floodplain} = \Big( \sum_{n=1}^{N} A_n R_n^{2/3} \Big) K \sqrt{S} \tag{19}$$

In many cases the roughness coefficient is also subdivided, but if you want to keep at in the calibration parameter, it should be considered as one value. It is possible to assume a certain ratio between the roughness in the main channel and floodplain, to have some more insights in the physical behaviour of the roughness as function of the water level.

Other limitations of the Manning's formula start to play a role when the flow becomes unsteady. These situations should be born in mind:

- At many locations, the discharge is not a unique function of stage; variables such as surface slope or rate of change of stage with respect to time must also be known to obtain the complete relationship in such circumstances. This led to adjustment in the rating curves to compensate for the unsteady flow. During fast rising water levels the water surface slope is significantly steeper than for steady flow conditions, resulting in greater discharge than indicated by the steady flow conditions. The rating curve will not be a unique relation between water level and discharge, but it will show loopings for the rising and falling water levels: hysteresis effects. This phenomena is most common in flat sloped rivers and rapid water level changes. Whether this occurs, can be determined by the Jones equation (Jones, 1916)

$$Q = Q_{steady} * \sqrt{1 + \frac{1}{Sc}\frac{\partial h}{\partial t}} \tag{20}$$

where $Q$ is the actual discharge, $Q_s teady$ is the discharge during steady flow, $S$ is the water surface slope, $c$ is the propagation speed of a high-water wave and $\frac{\partial h}{\partial t}$ is the change in water level in time

- Effect of backwater curves from the Zambezi river could also affect the the steady flow assumption. These effects are only mentioned a certain distance from the confluence. The effect slowly fades out and can be described by the Bélanger equation:

$$\frac{\partial h}{\partial x} = i_b \frac{h^3 - h_e^3}{h^3 - h_c^3} \tag{21}$$

where $\partial h/\partial x$ the spatial water depth gradient, $h$ the actual water depth and $h_g$ the critical water depth. The order of magnitude of the influence of those backwater curves is approx 1 till 100 kilometres.

## 8.2 Other recommendations

There are several ways to reconstruct 3D surface maps, but the use of stereophotogrammetry has many advantages; low-cost equipment, short time in the field and very user-friendly. A disadvantage, which is already mentioned in the discussion, is that the reconstruction is based on pixels and therefore vegetation is also included. LiDAR has got the major advantage that the laser beam is able to penetrate vegetation through canopy gaps, but these methods are also much more expensive.

The whole geometric profile of a river reach can be mapped during dry seasons, but to reconstruct a reliable physic-based rating curve you still need discharge measurements to calibrate it. An ADCP is one option to measure discharges in rivers, however it requires an expensive current meter and a boat. Remote areas, like several gauging stations in this research, are hardly accessible with the required equipment to execute measurements. Another method to determine discharges in rivers is by using the water surface velocity, which can be measured with Particle Image Velocimetry (PIV) technique (Detert & Weitbrecht, 2015; Johnson & Cowen, 2016). The fundamental concept of PIV involves tracking the displacement of patterns of small passive particles between two images, separated by a time interval. The next step is to convert the water surface velocity to depth averaged velocities, which is rather complicated. But if this relationship is established, the discharges can be calculated by knowing the geometric profile.

The principles of this method is to monitor the displacement of tracers added to the river in order to carry out an analysis of the spatial velocity in the river. Recently, significant efforts have been made to extend PIV to UAV, where the main advantage is the ability to rapidly characterize water flow systems in relatively large areas (Detert & Weitbrecht, 2015). Another advantage of an UAV is that it allows non-contact measurements of surface velocity in river which are inaccessible, e.g. during a flood event, which make fixed measurement implementations impractical. So this also may give insights in the discharges during floods and the physic-based rating curve may be calibrated for high flow circumstances.

During a fieldtrip we tested this method and we used bottles, partly filled with sand, as tracers. Several things went wrong during this testcase. First, the tracers were hardly visible on a small phone screen, where a live streaming video was displayed. Because of this, it was difficult to see if the tracers were captured by the camera and the determination of the flight path. Secondly, there was not sufficient contrast between the tracers and the water. Riples and turbulent flow are continuously changing the environment around the tracers. The changing environment contains multiple colours, which should not be the same as the tracers in order to carry out an analysis.

# References

., P. (2014). *Algorithms used in photoscan (last accessed 26-03-2016).* http://www.agisoft.ru/forum/index.php?topic=89.0.

Abernethy, C. L. (2001). *Intersectoral management of river basins. proceedings of an international workshop on integrated water management in water-stressed river basins in developing countries: Strategies for poverty alleviation and agricultural growth, loskop dam, south africa, 16-21 october 2000* (Conference Proceedings). International Water Management Institute. Retrieved from `http://EconPapers.repec.org/RePEc:iwt:conprc:h029109`

Agisoft photoscan user manual (Professional Edition, Version 1.3 ed.) [Computer software manual]. (2017).

Alsdorf, D. E., Rodríguez, E. & Lettenmaier, D. P. (2007). Measuring surface water from space. *Reviews of Geophysics*, *45*(2), n/a–n/a. Retrieved from `http://dx.doi.org/10.1029/2006RG000197` (RG2002) doi: 10.1029/2006RG000197

Bemis, S. P., Micklethwaite, S., Turner, D., James, M. R., Akciz, S., Thiele, S. T. & Bangash, H. A. (2014). Ground-based and uav-based photogrammetry: A multi-scale, high-resolution mapping tool for structural geology and paleoseismology. *Journal of Structural Geology*, *69, Part A*, 163 - 178. Retrieved from `http://www.sciencedirect.com/science/article/pii/S0191814114002429` doi: http://dx.doi.org/10.1016/j.jsg.2014.10.007

Benson, M. A. & Dalrymple, T. (1967). *General field and office procedures for indirect discharge measurements* [Book; Book/Illustrated]. Washington, D.C. : U.S. Govt. Print. Off. (Includes bibliographical references)

Brown, K. (2002). Water scarcity: Forecasting the future with spotty data. *Science*, *297*(5583), 926–927. Retrieved from `http://science.sciencemag.org/content/297/5583/926` doi: 10.1126/science.297.5583.926

Chow, V. (1959). Open-channel hydraulics. *McGraw-Hill, New York City, New York.*

Dall'Asta, E. & Roncella, R. (2014, June). A comparison of semiglobal and local dense matching algorithms for surface reconstruction. *ISPRS - International Archives of the Photogrammetry, Remote Sensing and Spatial Information Sciences*, 187-194. doi: 10.5194/isprsarchives-XL-5-187-2014

Detert, M. & Weitbrecht, V. (2015). A low-cost airborne velocimetry system: proof of concept. *Journal of Hydraulic Research*, *53*(4), 532-539. Retrieved from `http://dx.doi.org/10.1080/00221686.2015.1054322` doi: 10.1080/00221686.2015.1054322

Di Baldassarre, G. & Claps, P. (2011). A hydraulic study on the applicability of flood rating curves. *Hydrology Research*, *42*(1), 10–19. Retrieved from `http://hr.iwaponline.com/content/42/1/10` doi: 10.2166/nh.2010.098

Freer, J., McMillan, H., McDonnell, J. & Beven, K. (2004). Constraining dynamic {TOPMODEL} responses for imprecise water table information using fuzzy rule based performance measures. *Journal of Hydrology*, *291*(3–4), 254 - 277. Retrieved from `http://www.sciencedirect.com/science/article/pii/S0022169404000356` (Catchment modelling: Towards an improved representation of the hydrological processes in real-world model applications) doi: http://dx.doi.org/10.1016/j.jhydrol.2003.12.037

Grauman, K. & Leibe, B. (2011, 4). Visual object recognition. In *Visual object recognition* (Vol. 11, pp. 1–180). doi: 10.2200/S00332ED1V01Y201103AIM011

Hamilton, A. & Moore, R. (2012). Quantifying uncertainty in streamflow records. *Canadian Water Resources Journal / Revue canadienne des ressources hydriques*, *37*(1), 3-21. Retrieved from `http://dx.doi.org/10.4296/cwrj3701865` doi: 10.4296/cwrj3701865

Johnson, E. & Cowen, E. (2016, 02). Remote monitoring of volumetric discharge employing bathymetry determined from surface turbulence metrics. , *52*.

Jones, B. E. (1916). A method of correcting river discharge for a changing stage. *US Geol. Survey Water Supply Paper 375-E*.

Kennard, M. J., Mackay, S. J., Pusey, B. J., Olden, J. D. & Marsh, N. (2010). Quantifying uncertainty in estimation of hydrologic metrics for ecohydrological studies. *River Research and Applications*, *26*(2), 137–156. Retrieved from `http://dx.doi.org/10.1002/rra.1249` doi: 10.1002/rra.1249

Kuczera, G. (1996). Correlated rating curve error in flood frequency inference. *Water Resources Research*, *32(7)*(2119-2127).

Lane, E. W. (1995). Design of stable channels. *Trans. ASCE 120*, 1235-1260.

Lee-Lueng, F., Douglas, A., Rosemary, M. & Ernesto, R. (2013). Swot: The surface water and ocean topography mission. *Wide-swath altimetric measurement of water elevation on earth.*

Manning, R. (1891). On the flow of water in open channels and pipes. *Trans. Inst. Civ. Eng. Ire.*, *20*, 161-207.

Martin, D. & Weitbrecht, V. (2015). A low-cost airborne velocimetry system: proof of concept. *Journal of Hydraulic Research*, *53*(4), 532-539.

Parodi, U. & Ferraris, L. (2004). Influence of stage discharge relationship on the annual maximum discharge statistics. *Natural Hazards*, *31*(3), 603–611. Retrieved from `http://dx.doi.org/10.1023/B:NHAZ.0000024893.57284.0e` doi: 10.1023/B:NHAZ.0000024893.57284.0e

Petersen-Øverleir, Asgeir. (2014). Some challenges in hydrometry. *La Houille Blanche*(4), 53-56. Retrieved from `https://doi.org/10.1051/lhb/2014038` doi: 10.1051/lhb/2014038

Petersen-Øverleir, A. (2006). Modelling stage—discharge relationships affected by hysteresis using the jones formula and nonlinear regression. *Hydrological Sciences Journal*, *51*(3), 365-388. Retrieved from `http://dx.doi.org/10.1623/hysj.51.3.365` doi: 10.1623/hysj.51.3.365

Riggs, H. (1976). A simplified slope-area method for estimating flood discharges in natural channels. *Journal of Research of the United States Geological Survey 4*, 285-291.

Savenije, H. H. (2003). The width of a bankfull channel; lacey's formula explained. *Journal of Hydrology*, *276*(1), 176 - 183. Retrieved from `http://www.sciencedirect.com/science/article/pii/S0022169403000696` doi: http://dx.doi.org/10.1016/S0022-1694(03)00069-6

Schaefli, B., Harman, C. J., Sivapalan, M. & Schymanski, S. J. (2011). Hess opinions: Hydrologic predictions in a changing environment: behavioral modeling. *Hydrol. Earth Syst. Sci.*, *15*, 635-646. doi: 10.5194/hess-15-635-2011

Sivapalan, M. (2003). Prediction in ungauged basins: a grand challenge for theoretical hydrology. *Hydrological Processes*, *17*(15), 3163–3170. Retrieved from `http://dx.doi.org/10.1002/hyp.5155` doi: 10.1002/hyp.5155

Smith, L. C. (1997). Satellite remote sensing of river inundation area, stage, and discharge: a review. *Hydrological Processes*, *11*(10), 1427–1439. Retrieved from `http://dx.doi.org/10.1002/(SICI)1099-1085(199708)11:10<1427::AID-HYP473>3.0.CO;2-S` doi: 10.1002/(SICI)1099-1085(199708)11:10<1427::AID-HYP473>3.0.CO;2-S

Stevens, J. (1907). A method of estimating stream discharge from a limited number of gaugings. *Engineering News*, *58*(3), 52-53.

Westoby, M., Brasington, J., Glasser, N., Hambrey, M. & Reynolds, J. (2012). 'structure-from-motion' photogrammetry: A low-cost, effective tool for geoscience applications. *Geomorphology*, *179*, 300 - 314. Retrieved from `http://www.sciencedirect.com/science/article/pii/S0169555X12004217` doi: http://dx.doi.org/10.1016/j.geomorph.2012.08.021

Yan, K., Di Baldassarre, G., Solomatine, D. P. & Schumann, G. J.-P. (2015). A review of low-cost spaceborne data for flood modelling: topography, flood extent and water level. *Hydrological Processes*, *29*(15), 3368–3387. Retrieved from `http://dx.doi.org/10.1002/hyp.10449` (HYP-14-0542.R1) doi: 10.1002/hyp.10449

Yen, B. (1991). Hydraulic resistance in open channels. *Water Resources Publications, Highlands, Colorado,*, 1-118.

# A Flight maps

This part of the Appendix shows the flight maps that are flown with the Drone. Attempts where made to fly perpendicular to the river to obtain a rectangular map. This is desirable for the terrain analysis, because the DEM will be shaped to a rectangular map and in this way the DEM can be used as efficiently as possible.



(a) Mushumbi Bridge
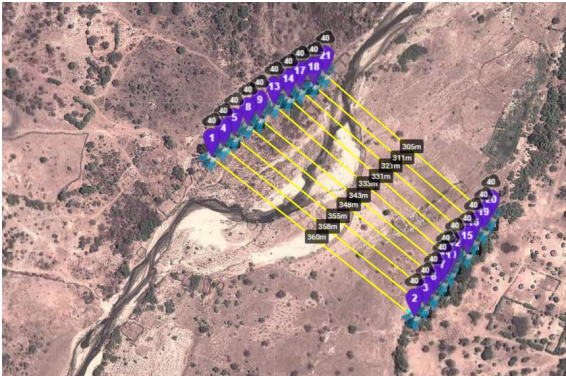


(b) Nyambudzi School

Figure A.1: Flight paths over the Manyame river

(a) Muzarabani Bridge
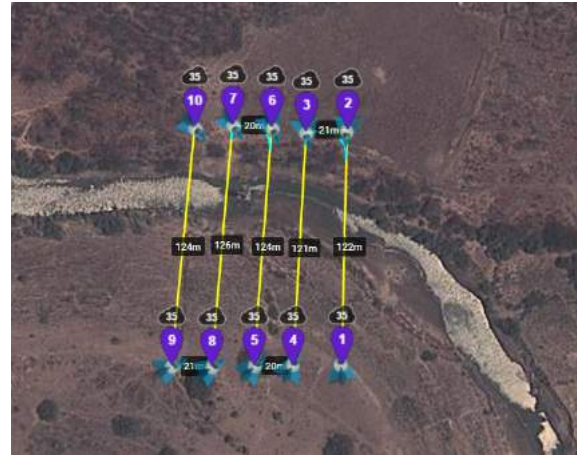


(b) Chidodo

Figure A.2: Flight paths over the Muzengesi river



Figure A.3: Flight path over the Angwa river at Angwa Bridge

# B    RMSE of Ground Control Points

The following pictures show the Root Mean Squared Errors of the GCP distributed over the floodplains over the rivers. A map of the locations of the GCP is shown, included the horizontal error by means of an ecliptic plane. The error in the elevation is indicated by means of the color of this ecliptic plane and the scale bar can be seen on the right side. More specified information about he errors can be find in the tables.

## Mushumbi Bridge
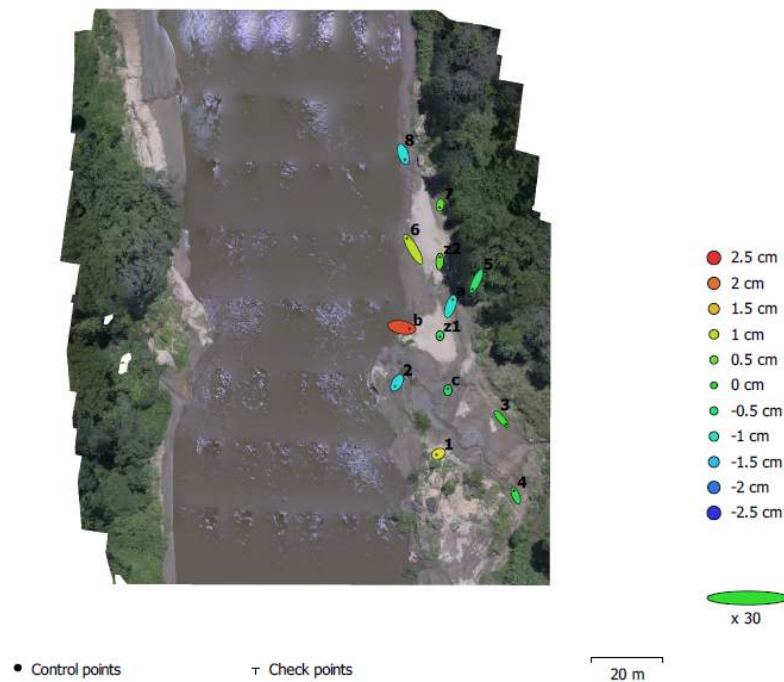


Figure B.1: GCP locations and error estimates: Z error is represented by ellipse color. X,Y errors are represented by ellipse shape. Estimated GCP locations are marked with a dot or crossing.

| Label | X error (cm) | Y error (cm) | Z error (cm) | Total (cm) | Image (pix) |
|---|---|---|---|---|---|
| 4 | -3.69514 | 8.97066 | -0.207232 | 9.70411 | 0.188 (16) |
| a | 4.30709 | 12.2775 | -1.14863 | 13.0617 | 0.462 (12) |
| 2 | -3.85186 | -6.60003 | -1.30297 | 7.75209 | 0.391 (15) |
| c | 0.148581 | 2.79331 | -0.449016 | 2.83307 | 0.520 (13) |
| 3 | 8.35486 | -10.1725 | 0.0068104 | 13.1637 | 0.274 (16) |
| z1 | 0.028861 | -1.7939 | -0.382273 | 1.8344 | 0.275 (16) |
| z2 | 0.417744 | 8.3296 | 0.343275 | 8.34713 | 0.390 (12) |
| b | 14.1074 | -2.45458 | 2.29987 | 14.5029 | 0.320 (17) |
| 6 | -11.7076 | 20.1665 | 0.97423 | 23.3389 | 0.349 (12) |
| 7 | -0.82194 | -4.4805 | 0.338431 | 4.56782 | 0.219 (16) |
| 8 | 3.41389 | -10.0824 | -1.22405 | 10.7149 | 0.080 (18) |
| 5 | -7.26386 | -15.1842 | -0.458658 | 16.8385 | 0.248 (12) |
| 1 | -3.47933 | -1.70292 | 1.24971 | 4.07031 | 0.288 (12) |
| **Total** | **6.38707** | **9.71341** | **1.00572** | **11.6686** | **0.319** |

Figure B.2: Root mean square error for X, Y and Z coordinates for all GCP location and the total error, which implies averaging over all the GCP locations

## Angwa Bridge
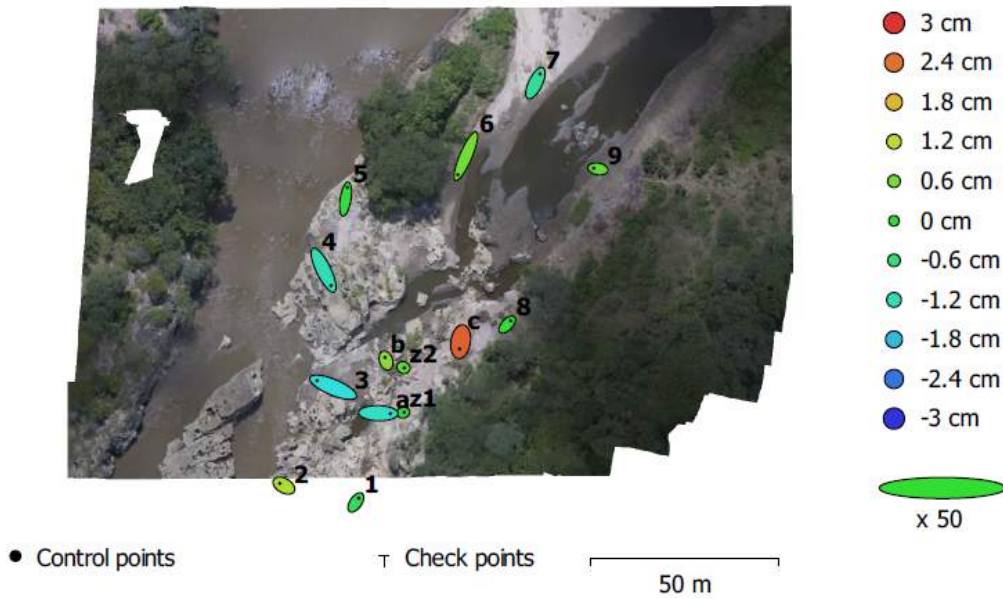


Figure B.3: GCP locations and error estimates: Z error is represented by ellipse color. X,Y errors are represented by ellipse shape. Estimated GCP locations are marked with a dot or crossing.

| Label | X error (cm) | Y error (cm) | Z error (cm) | Total (cm) | Image (pix) |
|-------|--------------|--------------|--------------|------------|-------------|
| 1 | 3.06391 | 4.47968 | -0.348798 | 5.43845 | 0.174 (8) |
| 2 | -4.33514 | 2.39716 | 1.07665 | 5.06942 | 0.163 (8) |
| 4 | 7.94006 | -16.2308 | -1.13623 | 18.1046 | 0.167 (20) |
| 3 | -17.0006 | 7.05929 | -1.51588 | 18.4703 | 0.182 (21) |
| z2 | 0.863226 | -0.36998 | 0.349782 | 1.00219 | 0.566 (29) |
| z1 | 1.04852 | 0.204259 | -0.13748 | 1.07704 | 0.391 (24) |
| b | -1.08774 | 3.24871 | 0.761239 | 3.50952 | 0.281 (28) |
| c | -1.16191 | -7.65518 | 2.55401 | 8.15321 | 0.283 (27) |
| a | 12.8838 | -0.372283 | -1.33576 | 12.9582 | 0.475 (26) |
| 5 | 2.0146 | 12.408 | -0.0949722 | 12.5709 | 0.156 (18) |
| 6 | -8.38862 | -19.6633 | 0.528711 | 21.3845 | 0.194 (19) |
| 8 | 3.84743 | 3.97374 | -0.112059 | 5.53226 | 0.171 (26) |
| 7 | 4.81694 | 9.86255 | -0.913404 | 11.0139 | 0.079 (19) |
| 9 | -4.53563 | 0.744147 | 0.356655 | 4.61009 | 0.114 (26) |
| **Total** | **6.98786** | **8.7128** | **1.04062** | **11.2172** | **0.302** |

Figure B.4: Root mean square error for X, Y and Z coordinates for all GCP location and the total error, which implies averaging over all the GCP locations

# Muzarabani Bridge
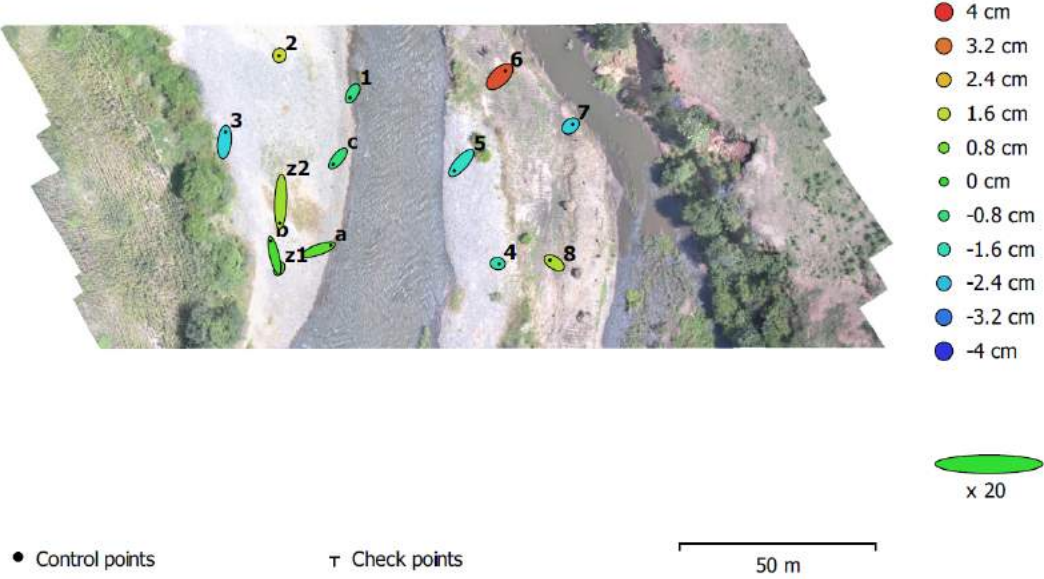


Figure B.5: GCP locations and error estimates: Z error is represented by ellipse color. X,Y errors are represented by ellipse shape. Estimated GCP locations are marked with a dot or crossing.

| Label | X error (cm) | Y error (cm) | Z error (cm) | Total (cm) | Image (pix) |
|-------|--------------|--------------|--------------|------------|-------------|
| 5 | -18.5611 | -20.3303 | -1.7849 | 27.5867 | 0.414 (19) |
| 7 | 5.44996 | 4.39985 | -2.15731 | 7.32903 | 0.318 (16) |
| 8 | -10.8507 | 7.28467 | 1.44679 | 13.149 | 0.357 (17) |
| a | 30.7809 | 10.6846 | 0.474587 | 32.5861 | 0.742 (19) |
| z1 | 2.18535 | 4.72621 | 0.616689 | 5.24339 | 0.571 (15) |
| 6 | 14.8956 | 14.4255 | 3.63227 | 21.0515 | 0.188 (14) |
| 4 | 3.73157 | -0.678564 | -1.47962 | 4.07116 | 0.439 (15) |
| b | -9.07331 | 36.7641 | 0.216409 | 37.8678 | 0.425 (16) |
| z2 | -2.08405 | -54.9549 | 1.20958 | 55.0077 | 0.439 (17) |
| 2 | -0.486309 | -1.34073 | 1.7718 | 2.2745 | 0.561 (16) |
| 1 | -6.38474 | -11.1223 | -0.965557 | 12.8609 | 1.009 (18) |
| c | -12.372 | -14.8154 | -0.80428 | 19.3187 | 0.808 (16) |
| 3 | 2.77808 | 24.9862 | -2.11547 | 25.2291 | 0.408 (17) |
| **Total** | **12.3053** | **21.7888** | **1.67848** | **25.0796** | **0.565** |

Figure B.6: Root mean square error for X, Y and Z coordinates for all GCP location and the total error, which implies averaging over all the GCP locations

# Chidodo
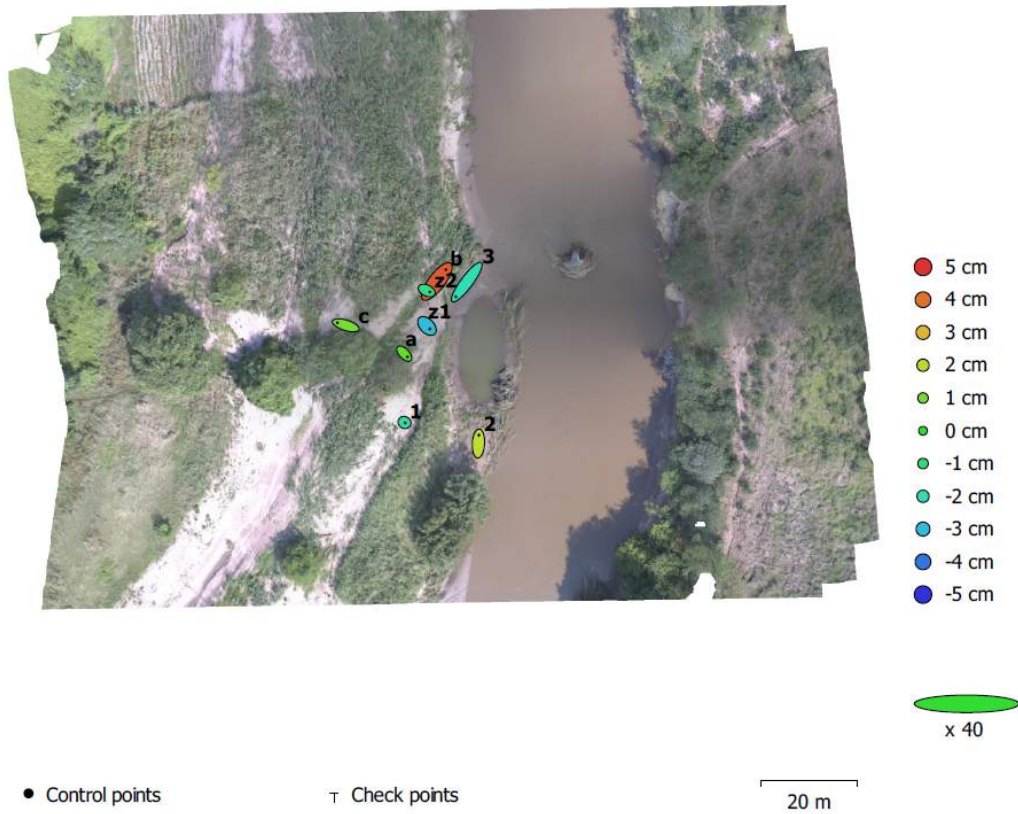


Figure B.7: GCP locations and error estimates: Z error is represented by ellipse color. X,Y errors are represented by ellipse shape. Estimated GCP locations are marked with a dot or crossing.

| Label | X error (cm) | Y error (cm) | Z error (cm) | Total (cm) | Image (pix) |
|-------|--------------|--------------|--------------|------------|-------------|
| b | 9.2674 | 12.1583 | 4.32065 | 15.8863 | 0.155 (24) |
| z1 | 2.99597 | -3.08552 | -3.03501 | 5.26379 | 0.399 (17) |
| 3 | -11.3042 | -15.1664 | -1.89536 | 19.0104 | 0.365 (18) |
| 2 | 0.446337 | 8.60377 | 2.03342 | 8.85205 | 0.265 (19) |
| z2 | 3.32627 | -1.55977 | -1.30222 | 3.89779 | 0.171 (17) |
| 1 | 0.637663 | -0.324236 | -1.77816 | 1.91667 | 0.381 (17) |
| c | -8.6181 | 2.67287 | 0.989529 | 9.07717 | 0.233 (18) |
| a | 3.24006 | -3.3395 | 0.641167 | 4.69694 | 0.941 (14) |
| **Total** | **6.31551** | **7.76387** | **2.28731** | **10.2662** | **0.403** |

Figure B.8: Root mean square error for X, Y and Z coordinates for all GCP location and the total error, which implies averaging over all the GCP locations

# Nyambudzi Bridge
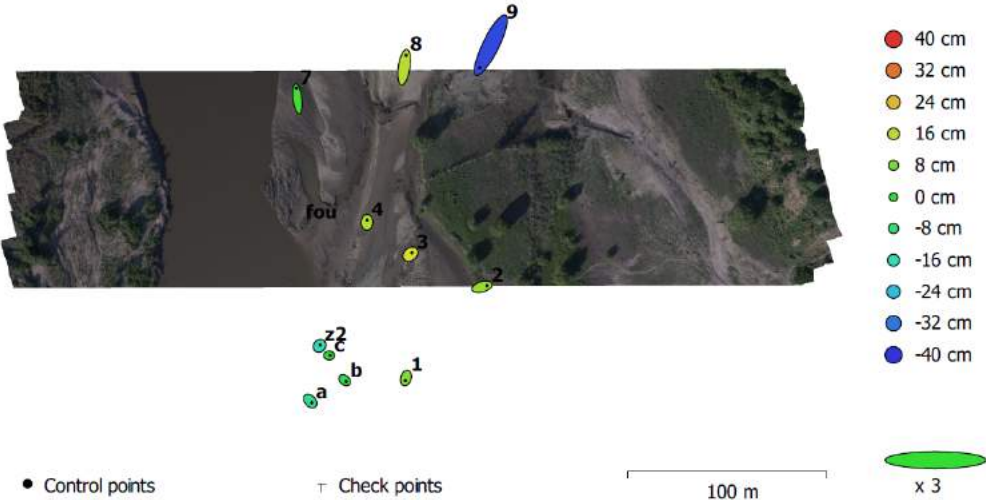


Figure B.9: GCP locations and error estimates: Z error is represented by ellipse color. X,Y errors are represented by ellipse shape. Estimated GCP locations are marked with a dot or crossing.

| Label | X error (m) | Y error (m) | Z error (m) | Total (m) | Image (pix) |
|-------|-------------|-------------|-------------|-----------|-------------|
| b | 0.474935 | -0.416782 | -0.0389781 | 0.63308 | 0.000 (17) |
| c | 0.335758 | -0.0115318 | -0.0184017 | 0.33646 | 0.000 (16) |
| z2 | 0.190645 | 0.252664 | -0.157599 | 0.353585 | 0.000 (17) |
| 7 | -0.418185 | 3.55608 | 0.0158441 | 3.58062 | 0.000 (16) |
| a | 0.6101 | -0.594106 | -0.119229 | 0.859884 | 0.000 (14) |
| 1 | -0.246709 | -0.870925 | 0.0927003 | 0.909928 | 0.000 (14) |
| 2 | 1.68368 | 0.504699 | 0.114166 | 1.7614 | 0.000 (13) |
| 4 | 0.0267363 | 0.706541 | 0.149493 | 0.722678 | 0.000 (18) |
| 3 | 0.522493 | 0.417867 | 0.190632 | 0.695667 | 0.000 (19) |
| 9 | -3.78159 | -7.62222 | -0.378018 | 8.51713 | 0.000 (16) |
| 8 | 0.60552 | 4.07475 | 0.150772 | 4.12226 | 0.000 (14) |
| **Total** | **1.30587** | **2.85442** | **0.161557** | **3.14311** | **0.000** |

Figure B.10: Root mean square error for X, Y and Z coordinates for all GCP location and the total error, which implies averaging over all the GCP locations

# C    Digital Elevation Maps
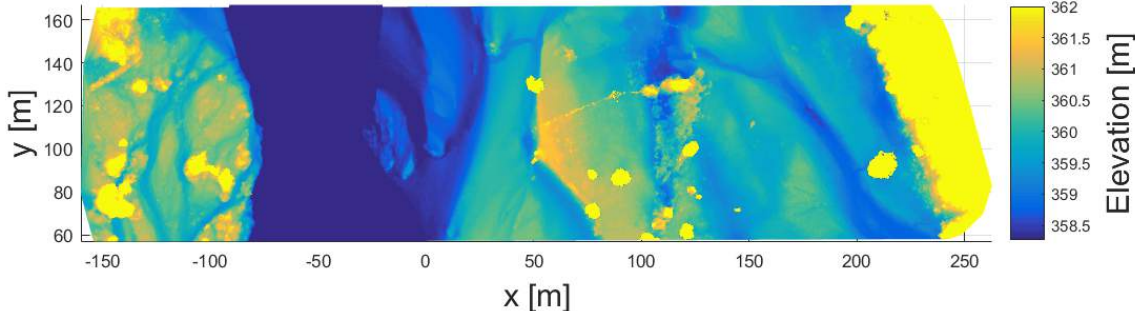


Figure C.1: Digital Elevation Maps of Gauging station Nyambudzi School
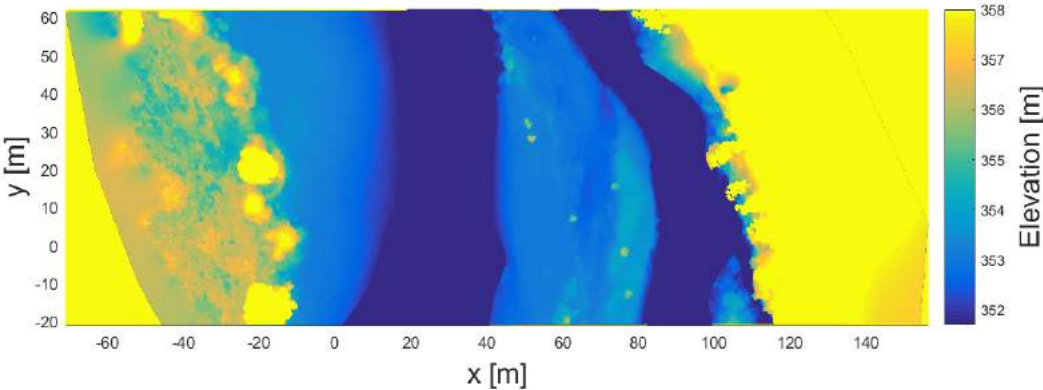


Figure C.2: Digital Elevation Maps of Gauging station Muzarabani Bridge
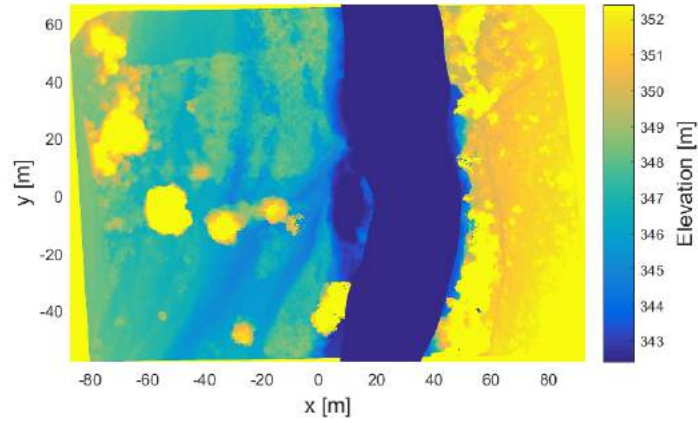
Figure C.3: Digital Elevation Maps of Gauging station Chidodo

# D    Reach-averaged cross-sectional parameters
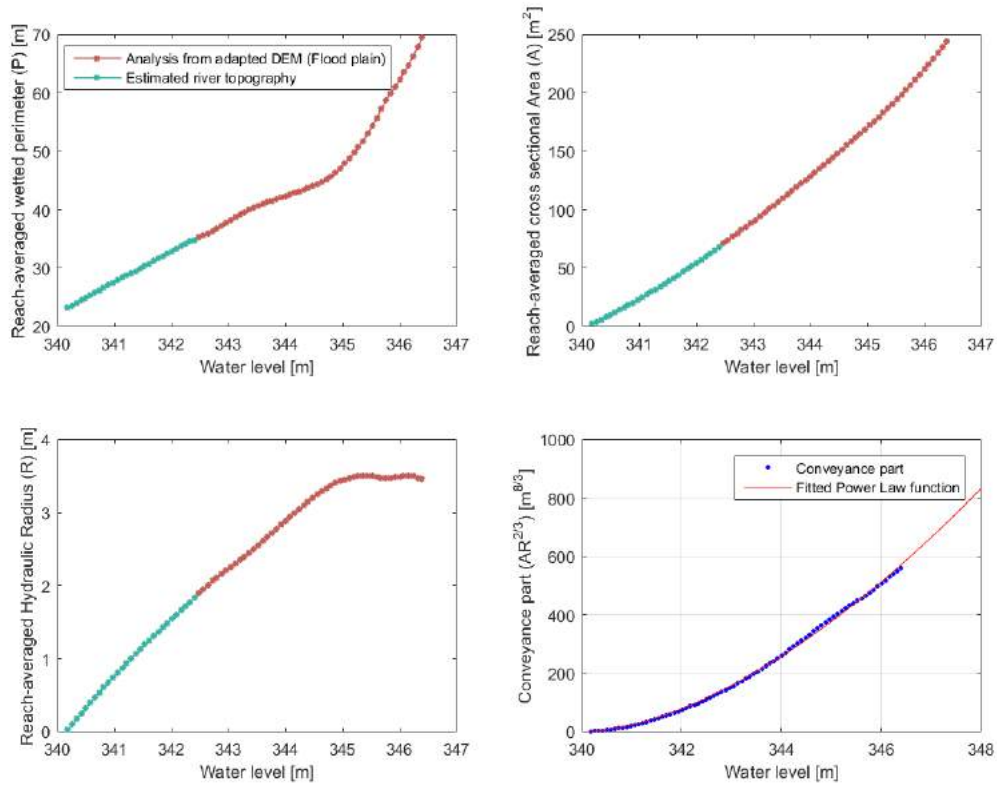


Figure D.1: Cross-sectional parameters at Chidodo, where the river topography is estimated (described in section 4.2). Left upper corner: Wetted perimter - water level relationship. Left lower corner: Hydraulic Radius - water level relationship. Right upper corner: Cross sectional area - water level relationship. Right lower corner: Conveyance- water level relationship.
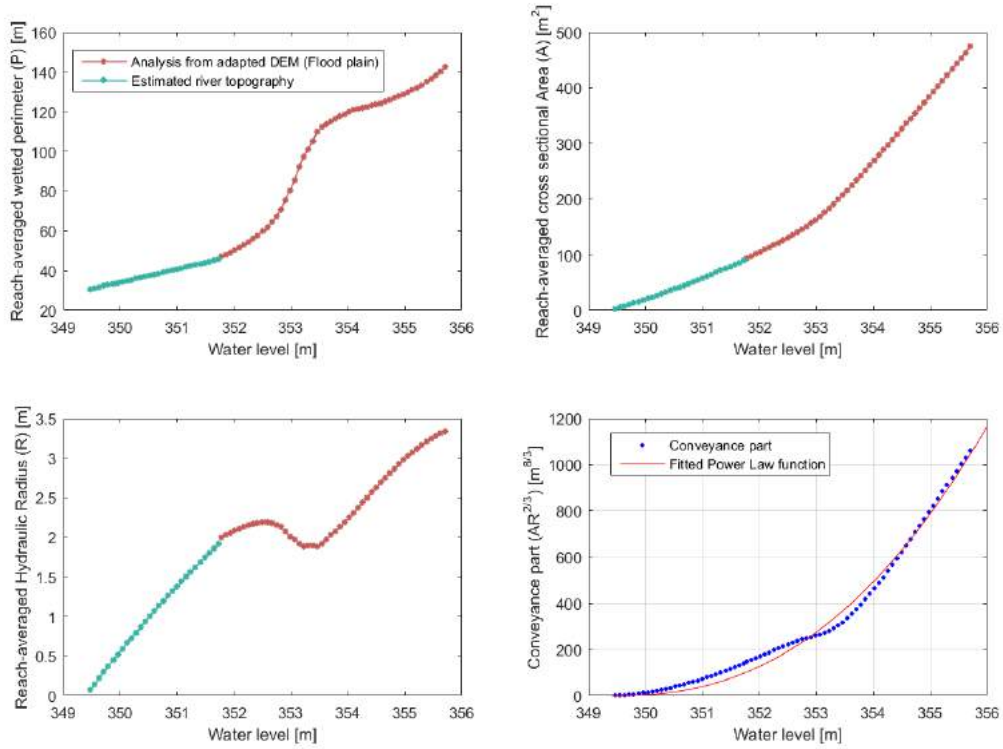
Figure D.2: Cross-sectional parameters at Muzarabani bridge, where the river topography is estimated (described in section 4.2). Left upper corner: Wetted perimter - water level relationship. Left lower corner: Hydraulic Radius - water level relationship. Right upper corner: Cross sectional area - water level relationship. Right lower corner: Conveyance- water level relationship.
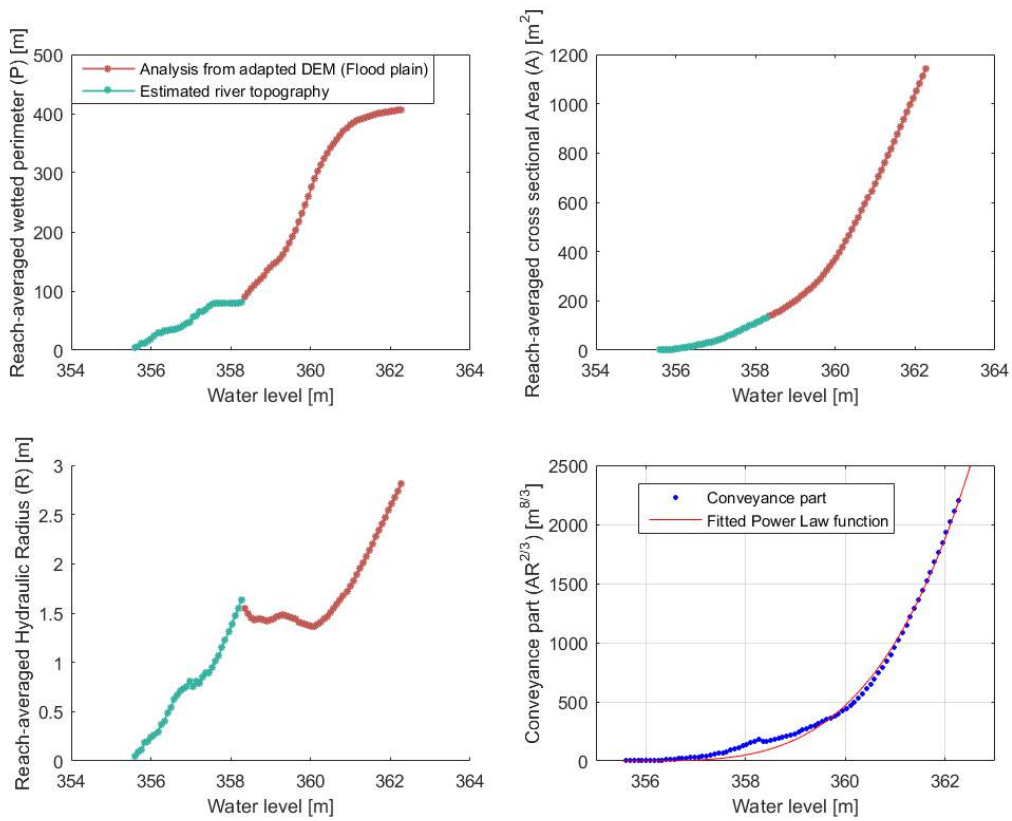
Figure D.3: Cross-sectional parameters at Nyambudzi School, where an ADCP measurement was done for the river topography. Left upper corner: Wetted perimter - water level relationship. Left lower corner: Hydraulic Radius - water level relationship. Right upper corner: Cross sectional area - water level relationship. Right lower corner: Conveyance- water level relationship.